Journal of Hydrology 603 (2021) 126912

Contents lists available at ScienceDirect

Journal of Hydrology

journal homepage: www.elsevier.com/locate/jhydrol

Research papers

Temperature distribution in coastal aquifers: Insights from groundwater modeling and field data

A.M. Blanco-Coronas [a,*], C. Duque [b], M.L. Calvache [a], M. López-Chicano [a]

[a] Departamento de Geodinámica, Universidad de Granada, Avenida Fuente Nueva s/n, 18071 Granada, Spain
[b] WATEC, Department of Geoscience, Aarhus University, Høegh-Guldbergs Gade 2, 8000 Aarhus C, Denmark

ARTICLE INFO

This manuscript was handled by Corrado Corradini, Editor-in-Chief, with the assistance of Stephen Worthington, Associate Editor

Keywords:
Heat transport
Numerical modeling
Geothermal gradient
Saltwater intrusion
Temperature fluctuations

ABSTRACT

The temperature distribution in coastal aquifers is determined by the effect of different heat sources: surface water recharge, sea infiltration, and geothermal heat. In previous studies, the signal generated in groundwater by each source was individually studied, and in the case of geothermal heat, it was often not considered. This research is the first in considering all possible sources of heat in a coastal aquifer simultaneously by using a combination of field data and numerical modeling to present a reference model based on the characteristics of a real aquifer. The position of the freshwater-saltwater interface (FSI) and its effect on temperature distribution have been modeled considering variable-density flow, coupled heat and solute transport. This study broadens the theoretical knowledge of temperature distribution in coastal aquifers based on a sensitivity analysis of hydraulic and thermic parameters. Furthermore, a case study (the Motril-Salobreña aquifer) was modeled with field data calibration to test the applicability to real aquifers. The new insights gained through this study provide integrated knowledge of the temperature distribution in coastal areas and establish the basis for future research using heat as a tracer in seaside aquifers.

1. Introduction

The use of heat as a groundwater tracer is growing in popularity and it has been extended in a wide range of hydrogeological studies (Anderson, 2005). Heat and solute transport have many similarities (deMarsily, 1986; Bear, 1972; Hopmans et al., 2002), which is the reason heat has been used as a tracer in groundwater systems. However, there are also differences in their behavior (Vandenbohede et al., 2009; Ma et al., 2012) due to the thermal exchange between water and aquifer solids, which depends on the heat properties of both (Bakker et al., 2015). This reflects a time delay of heat transport with respect to solute transport. For this reason, understanding the different aspects involved in both processes is important when including both solute transport and heat transport in the same model. Traditionally, the direct relationship of density and viscosity with temperature has been ignored in hydrogeological modeling because of its negligible effect over the results of variable density models; nevertheless, there is a broad area of research in groundwater systems where temperature is considered to play a significant role (e.g., sole-source aquifers and coastal aquifer/ocean interactions) (Thorne et al., 2006; Vandenbohede and Van Houtte, 2012; Befus et al., 2013; Debnath et al., 2005).

Studies about groundwater-surface water interaction have shown that thermal distribution in the aquifer can indicate the degree of connection with rivers that has seasonal and daily temperature fluctuations (Constantz, 1998; Duque et al., 2010; Keery et al., 2007; Lautz, 2012; McCallum et al., 2014; Sebok et al., 2015). Recharge processes can have an impact on temperature of the surficial zone of the aquifer to a maximum depth of a few tens of meters as a consequence of atmospheric temperature (Pollack and Huang, 2000; Smerdon et al. 2003). Variations in environmental temperature produce groundwater temperature fluctuations due to the effect of cooling or heating of the surface water before infiltration (Pollack et al., 2005; Duque et al., 2010). The amplitude of fluctuations decreases with depth (Silliman and Booth, 1993; Kurylyk et al., 2013). As a result, the thermal signal has been used in analytical and numerical solutions to estimate groundwater recharge/discharge rates (Suzuki, 1960; Bredehoeft and Papadopulos, 1965; Stallman, 1965; Rushton, 2007; Duque et al., 2016). Taniguchi et al. (1999), Calvache et al. (2011), and Kurylyk et al. (2019) have described how the shape of temperature profiles is connected with discharge and recharge areas.

* Corresponding author.
E-mail addresses: ablanco@ugr.es (A.M. Blanco-Coronas), cduque@geo.au.dk (C. Duque), calvache@ugr.es (M.L. Calvache), mlopezc@ugr.es (M. López-Chicano).

https://doi.org/10.1016/j.jhydrol.2021.126912
Received 26 April 2021; Received in revised form 30 July 2021; Accepted 1 September 2021
Available online 8 September 2021

Apart from the surficial zone where temperature is affected by recharge and air temperature, aquifers can be affected by the geothermal gradient (Parsons, 1970). Temperature profiles within the geothermal zone are unaffected by seasonal variations and adopt a linear trend (Anderson, 2005). Domenico and Palciauskas (1973) indicated that the distribution of groundwater temperature can be disturbed by groundwater flow, and Stallman (1963) suggested that it depends directly on the velocity and direction of water flow. The geothermal gradient is greater in groundwater discharge areas than in recharge areas (Tóth, 1962; Domenico and Palciauskas, 1973; An et al., 2015), which results from the fact that a hot upwelling is forced by convection within the discharge zone (Szijártó et al., 2019). Hydraulic conductivity also plays an important role in the geothermal gradient, due to the high degree of convective heat transport with large hydraulic conductivity values (An et al., 2015). Other parameters such as anisotropy, heterogeneity, recharge rate, and the position of the water table have an important influence on the magnitude of the disturbance (Parsons, 1970; Smith and Chapman, 1983; Woodbury and Smith, 1988; Forster and Smith, 1989).

The groundwater flow pattern of coastal aquifers was initially studied in the 1950's and 1960's (Glover, 1959; Kohout, 1964). The intrusion of saline water into the deepest part of aquifers disturbs the freshwater flow due to the difference in density of the two fluids. Groundwater originated by recharge inland flows vertically upward resulting in fresh/terrestrial submarine groundwater discharge (SGD) across the seafloor, between land and sea. This process is intimately associated with the location of the freshwater-saltwater interface (FSI) and has been studied along many coasts of the world (Kinnear et al., 2013; Eissa et al., 2018; Duque et al., 2019; Zhang et al., 2020, Liu et al., 2021). Despite good knowledge about coastal areas, few studies have investigated heat distribution. A series of papers by the U.S. Geological Survey (USGS) in the 1960s hypothesized the existence of seawater circulation intensified by temperature-induced density gradients in a carbonate platform in southern of Florida (Kohout, 1965; Kohout, 1967; Henry and Kohout, 1972, Kohout et al. 1977). They hypothesized that infiltrated cold seawater could be heated by geothermal heat, driving to an open-cycle thermal convection in addition to variable-density effects. Subsequently, Henry and Kohout (1972) tested Kohout's thermal convection with a laboratory experiment. Cold saltwater and warm freshwater were introduced in a glass tank with sand. For the first time, a laboratory experiment represented combined solute and heat transport and their effects on flow patterns were represented in porous media. The Henry and Hilleke problem was modeled with different numerical codes, such as SUTRA-MS (Hughes et al., 2007), SEAWAT (Dausman et al., 2010), and HST3D (Thorne et al., 2006) showing very similar results among them. The same benchmark problem was used to simulate this physical experiment with SEAWAT but also included variable-density groundwater flow (Langevin et al., 2010). Nevertheless, there are only a few studies that support their hypothesis with field measurements, such as Kim et al. (2008, 2009) who described the dynamics within the freshwater-saltwater interface in a volcanic island with a geothermal gradient. The vertical logs in boreholes situated close to the coastline in an aquifer in southeastern of Spain (Molina et al., 2002) did not show a normal increase in temperature with depth but revealed a sharp decrease in temperature at −160 m depth due to the entry of cooler seawater into the aquifer. Furthermore, time-series data of electrical conductivity and temperature at different depths showed variations due to two external influences: tidal fluctuation and recharge produced by rainfall. Beyond this, Vandenbohede and Lebbe (2011) observed yearly fluctuations in temperature in the surficial zone of a shallow detrital coastal aquifer and developed a density-dependent model to simulate how yearly temperature oscillations influence the distribution of groundwater temperature. They concluded that the thickness of the surficial zone and the amplitude of the temperature oscillations are dependent on the conduction/convection dominance on heat transport.

In most cases, research has focused on either surficial temperature processes (Vandenbohede and Lebbe, 2011; Befus et al., 2013; Debnath et al., 2005; Tirado-Conde et al., 2019) or geothermal effects (Taniguchi, 2000; Taniguchi et al., 1999), as the distance between these effects hinders the exchange between them. In coastal aquifers, the circulation patterns generated due to variable density of the fluid and the hydrodynamic dispersion can facilitate the interaction between shallow and deep groundwater but research has been limited thus far to a few theoretical (e.g. Thorne et al., 2006; Langevin et al., 2007, 2008, 2010) or field measurements in all the depth of shallow aquifers but without detection of geothermal gradient (e.g. Folch et al., 2020). The difficulties in obtaining temperature data in deep zones of coastal areas originate the scarcity of research focused on the geothermal effect.

This paper shows the temperature distribution in coastal aquifers, distinguishes the different thermal zones that can be found in coastal areas, and takes into consideration constant or variable temperature sources over. For this purpose and due to the scarcity of information in the scientific literature, a numerical model was developed to propose a generic synthetic theoretical model of temperature distribution in coastal aquifers. A detailed sensitivity analysis was applied to different parameters and properties for a range of realistic values in the study area. The results established the basis for the understanding of heat distribution for diverse types of coastal aquifers. Furthermore, the acquired knowledge was tested with field data obtained in the coastal aquifer of Motril-Salobreña, making it one of the few studies that combined heat modeling with temperature field data obtained near the discharge zone.

2. Research area

2.1. Hydrogeological setting

The Motril-Salobreña detrital aquifer is located on the southeastern coast of Spain in the province of Granada (Fig. 1a). It has an area of 42 km^2, and its thickness varies from 30 to 50 m in the north to more than 250 m in the south (Duque et al., 2008). The aquifer is composed mostly of gravel, sand, silt, and clay of Quaternary age that overlay a very low permeability basement consisting of schist and phyllite (Fig. 1c). The hydraulic conductivity of the materials is widely variable (Calvache et al., 2015) due to the fluvial-deltaic depositional environment of the aquifer. In the vicinity of the mouth of the Guadalfeo River, the upper layers of the aquifer are characterized by gravel layers characterized by high hydraulic-conductivity; however, the ratio diminishes dramatically at a depth of 140 m due to the prevalence of clay layers (Fig. 1c). Numerical and sedimentological studies have estimated values of hydraulic conductivities, which ranged from 12 to 300 m/d (Calvache et al., 2009; Duque et al., 2018). The general flow direction in the aquifer is from north to south toward the Mediterranean Sea, with a hydraulic gradient estimated between 1.6×10^{-3} and 5×10^{-3} (Duque et al., 2010); although currently it reaches 7×10^{-3} in the northern part of the aquifer. The main water entrance to the aquifer is supplied by the Guadalfeo River, which provides direct infiltration along the riverbed and indirect infiltration from irrigation return flows, estimated at 11 Mm^3/year and 16 Mm^3/year, respectively (Calvache et al., 2009; Duque et al., 2011).

In the study area, several wells were drilled from north to south (W10, W250, W60, and W180) at distances of 285 m, 300 m, 700 m, and 1900 m from the shoreline (Fig. 1b). W10, W60, and W180 are three full-screened wells 10 m, 60 m, and 180 m deep respectively, and W250 is a deep well 250 m deep with one screen that is 6 m and 11 screens that are 3 m each at the depths indicated in Fig. 1c. W250 is an artesian well with an average flow of 18 L/s, providing evidence of the presence of vertical flows in this area of the aquifer (Calvache et al., 2015) according to the flow pattern of the discharge zone proposed by Glover (1959) and Kohout (1964) for a coastal aquifer. Duque et al. (2008) indicated slight marine intrusion in the aquifer by using gravitational and electromagnetic sounding methods, which were supported by the low electrical conductivity (EC) data obtained in W180. Additionally, well W250

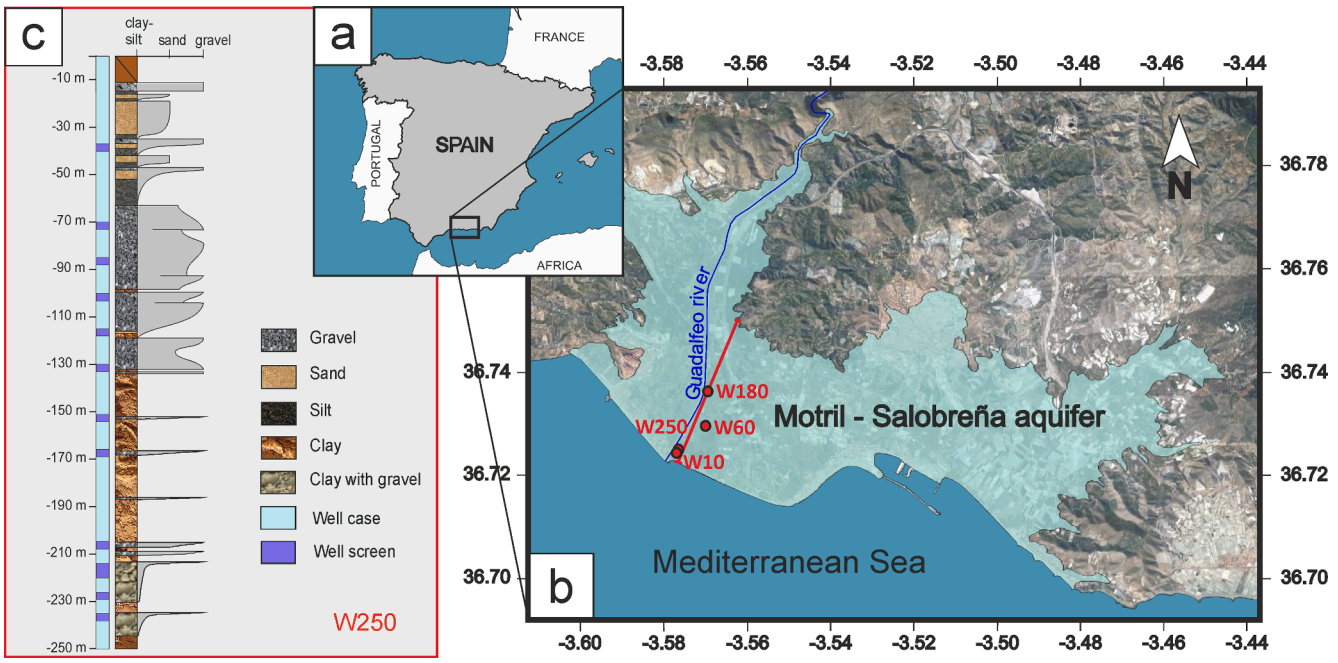

Fig. 1. (A) Location map of the research area; (B) Location of the Motril-Salobreña aquifer, research boreholes and cross section. (C) Lithological core of the W250 well and depths of the screens.

intersected the FSI, which was approximately 135–200 m deep (Calvache et al., 2015).

The area is characterized by a subtropical climate with scarce rainfall and mild temperature. The average precipitation is 420 mm/year, and the mean annual temperature is 18 °C. The mean air temperature follows a regular pattern each year: a maximum of 25 °C in July-August and a minimum of 10–12 °C in January-February (Duque et al., 2010). A similar pattern was observed in the temperature of water in the river with almost identical values to the atmospheric temperature but with an approximate delay of 1 month. On the other hand, the Mediterranean Sea in this area is characterized by a warm temperature that fluctuates between a maximum of 24 °C in August and a minimum of 14 °C in February (data supplied by the State Harbors, Spanish Ministry of Development). The temperature pattern in the upper section of the aquifer and in the proximity of the FSI was disturbed due to the influence of the thermal signal from the river (Duque et al., 2010) and the influence of the sea temperature respectively.

The collected data from well W180 represented the vertical heat distribution in the Motril-Salobreña aquifer (Fig. 2). Three zones can be identified: the surficial zone, intermediate zone, and deep zone. The surficial zone is subject to seasonal changes in temperature. The intermediate zone does not have any significant seasonal variations and remains practically constant. The deep zone has a constant increase in temperature due to geothermal heat.

2.2. Temperature conceptual model

The conceptual model (Fig. 3) was created from the field data information. The measurements obtained in W180 (Fig. 2) were used to establish the initial temperature distribution within the freshwater domain. A surficial zone 23 m deep with an oscillating thermal signal could be distinguished due to infiltration of the river flow and air temperature influence. Below the surficial zone, the intermediate zone is differentiated because temperature had no oscillations and remained at 17.2 °C until a depth of approximately 110 m. In the deep zone, an increment in temperature of 0.02 °C per meter was calculated, which represents 20 °C at −250 m. The temperature of the sea oscillated seasonally in the same manner as the temperature of the river flow. This

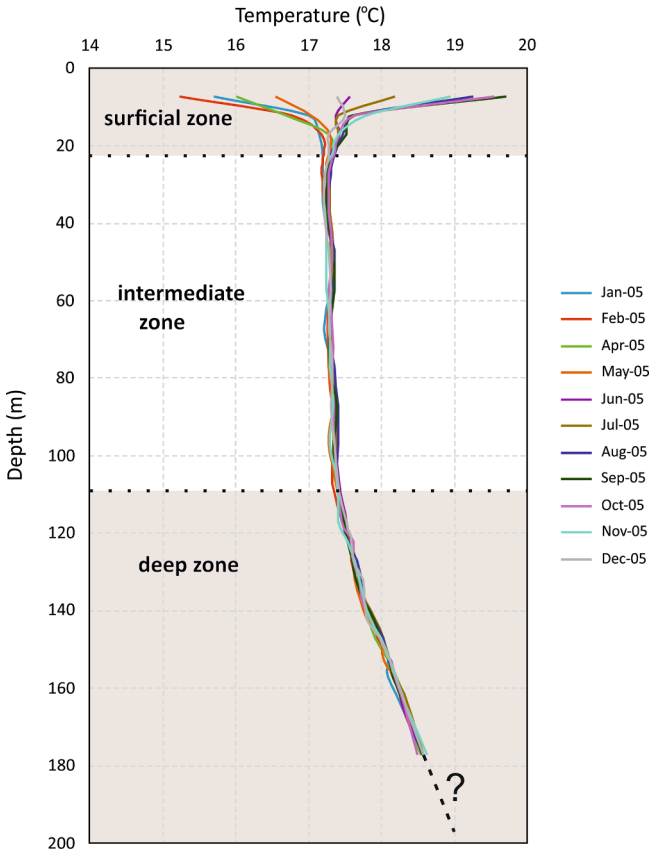

Fig. 2. Temperature vertical profiles measured in W180 collected monthly in 2005.

conceptualization was used for assigning boundary conditions in the numerical model, and temperature and head measurements in W10, W250 and W60 were used for calibration and verification of the model.

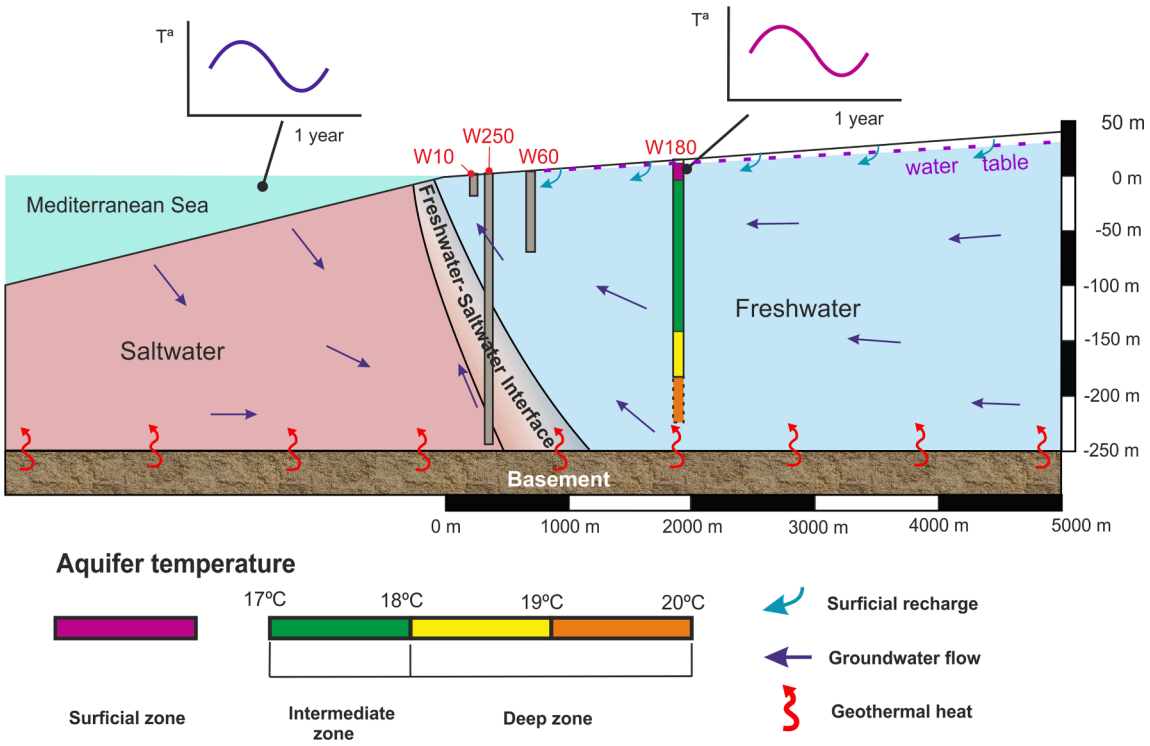

Fig. 3. Conceptual model of the temperature distribution of the Motril-Salobreña aquifer.

3. Methodology

3.1. Solute and heat transport equation, numerical model and model indicators

In the present study, SEAWAT v.4 (Langevin et al. 2007) was used to simulate simultaneous multispecies solute and heat transport. This software couples MODFLOW (Harbaugh et al., 2000) and MT3DMS (Zheng and Wang, 1999) and solves the following form of the variable-density groundwater flow equation:

$$\left(1+\frac{\rho_b K_d^k}{\theta}\right)\frac{\partial(\theta C^k)}{\partial t}=\nabla\left[\theta\left(D_m^k+\alpha\frac{q}{\theta}\right)\nabla C^k\right]-\nabla(qC^k)-q'_sC_s^k \quad (1)$$

where ρ_b is the bulk density (mass of the solids divided by the total volume) [ML-3], K_d^k is the distribution coefficient of species k [L^3M^{-1}], θ is porosity [-], C^k is the concentration of species k [ML^{-3}], t is time [t], D_m^k is the molecular diffusion coefficient [L^2t^{-1}] for species k, α is the dispersivity tensor [L], q is specific discharge [Lt^{-1}], q'_s is a fluid source or sink [t^{-1}], and C^k is the source or sink concentration [ML^{-3}] of species k. Dimensions include length [L], mass [M], time [t] and temperature [T].

Temperature is represented as one of the species of MT3DMS. Given that heat transport is analogous to solute transport in groundwater modeling, Thorne et al. (2006) adapted equation (1) to assign suitable thermal parameters for temperature species:

$$\left(1+\frac{1-\theta}{\theta}\frac{\rho_s}{\rho}\frac{C_{Psolid}}{C_{Pfluid}}\right)\frac{\partial(\theta T)}{\partial t}=\nabla\left[\theta\left(\frac{k_{Tbulk}}{\theta\rho c_{Pfluid}}+\alpha\frac{q}{\theta}\right)\nabla T\right]-\nabla(qT)-q'_sT_s \quad (2)$$

where ρ_s is the density of the solid (mass of the solid divided by the volume of the solid) [ML^{-3}], ρ is the fluid density [ML^{-3}], C_{Psolid} is the specific heat capacity of the solid [$L^2t^{-2}T^{-1}$], C_{Pfluid} is the specific heat capacity of the fluid [$L^2t^{-2}T^{-1}$], T is temperature [T], k_{Tbulk} is the bulk thermal conductivity of the aquifer material [$MLt^{-3}T^{-1}$] and T_s is source temperature [T]. Bulk density is calculated by $\rho_b = \rho_s(1-\theta)$.

Equations (1) and (2) show that heat transport is controlled by convection and conduction, which are mathematically equivalent to advection and diffusion for solute transport, respectively. Both transport equations incorporate a retardation term. The adsorption of solutes by the aquifer matrix generates retardation in solute transport, whereas the thermal transfer between the fluid and solid aquifer matrix produces retardation in heat transport. A linear sorption isotherm was applied to the model to represent the thermal retardation by calculating the distribution coefficient (K_d) for temperature species:

$$K_d^t=\frac{C_{Psolid}}{\rho C_{Pfluid}} \quad (3)$$

The thermal conduction term for temperature species D_m^T [L^2/T], is mathematically equivalent to molecular solute diffusion for the solute species. Heat and solute transfer are related to a gradient, from high-concentration areas to low-concentration areas. Bulk thermal diffusivity is calculated from the relationship between equations (1) and (2):

$$D_m^T=\frac{k_{Tbulk}}{\theta\rho c_{Pfluid}} \quad (4)$$

In turn, bulk thermal conductivity k_{Tbulk} is obtained solving the following equation (Hughes et al., 2007):

$$k_{Tbulk}=\theta k_{Tfluid}+(1-\theta)k_{Tsolid} \quad (5)$$

Thermal dispersion in heat transport is frequently ignored in most analytical solutions (Langevin et al., 2010) because heat conduction often dominates thermal dispersion in heat transport (Anderson, 2005; Ferguson, 2007). However, SEAWAT (version 4) includes the thermal dispersion term in the code formulation; therefore, it has been included in our models.

To interpret the temperature distribution within the aquifer and to quantitatively compare the model results, we used the following indicators:

1. $D(B,tc_i)$ is the vertical distance from the aquifer basement to each thermal contour:

$$D(B, tc_i) = -(Z_B - Z_{tc_i}) \quad (6)$$

2. R is the dimensionless factor obtained from the division of the vertical distance from sea surface level to each thermal contour and the location of the arbitrary observation point:

$$R = \frac{Z_{sl} - Z_{tc_i}}{X_{obs}} \quad (7)$$

where i is the temperature of the thermal contour [T], Z_B is the elevation of the aquifer basement [L] using sea level as a reference, Z_{tc_i} is the elevation of the thermal contour [L] using sea level as a reference, Z_{sl} is the elevation of sea level [L], and X_{obs} is the position of the observation point on the x-axis [L].

The root mean squared error (RMSE) was calculated on the basis of the comparison of the observed data with the field measurements:

The coefficient of determination (R^2) and the root mean squared error (RMSE) were calculated on the basis of the comparison of the observed data with the field measurements:

$$R^2 = 1 - \frac{\sum (T_m - T_s)}{\sum (T_m - \bar{T})}$$

$$RMSE = \sqrt{\frac{1}{n}\sum_{i=1}^{n} (T_m - T_s)^2}$$

where T_m is the measured temperature [T], T_s is the simulated temperature [T], $\bar{T}$ is the mean of the temperature values [T] and n is the number of observations.

3.2. Field data

Four research wells were used to study the temperature distribution of the aquifer. Vertical temperature profiles were logged monthly at W180 and, W60 and sporadically at W250 using the multiparameter probe KLL-Q-2 (accuracy: ±0.1 °C; resolution 0.01 °C) during the period 2005–2019. In W180, the profiles were obtained by measuring every five meters throughout the well. In W250, the measurement points of the logs were taken at the depths of the 12 screens (Fig. 1c). In W60, the observation points of the logs were obtained every 5 m to a depth of 20 m. In W10, one pressure–temperature sensor was installed at a 5-m depth to measure at 1-hour intervals (Seametrics LevelSCOUT smart pressure sensors; accuracy: ± 0.1 °C and resolution: ± 0.01 °C). The collection of temperature profiles is subject to uncertainties. Water circulation inside the casing of the well affects the temperature distribution and the measurements could not be an exact replica of temperature into the aquifer. However, as the objective of this research was to focus on the major trends and general dynamics, this limitation was considered acceptable. Other methodologies to collect temperature profiles such as fiber-optic distributed temperature sensing (FO-DTS) directly inserted in the aquifer sediments prevent the problem of water circulation inside wells (del Val et al., 2021) but it requires specific design and construction of the monitoring system instead of using boreholes already drilled. The temperature dataset of the Mediterranean Sea was supplied from monthly mean temperature by the State Harbors (Spanish Ministry of Development) on the coast at Málaga. This station was chosen because it was closer to the research area (75 km west) and because climatic conditions were practically the same: the same mean monthly temperature and mean precipitation. The measurement device was a TRIAXYS™ Directional Wave Buoy that measures temperature 0.5 m below the sea surface and provides real-time data via radio to a land station with hourly cadence.

3.3. Numerical model characteristics

The temperature distribution within the coastal aquifer was modeled with a finite-difference 2D model using SEAWAT, which solved the variable-density groundwater flow and heat transport equations. The 2D model (cross-section) was 8.5 km long (x-axis), of which 5 km were landward and 3.5 km seaward from the coastline, and 100 m wide (y-axis). The depth of the model (z-axis) varied from 150 m in the south (offshore boundary) to 290 m deep in the north (onshore boundary). The topography of the aquifer and seabed had slopes of 0.8% and 2.8% respectively, based on a groundwater age model of the study area (Calvache et al., 2020) and the seabed bathymetric information (Jabaloy-Sánchez et al., 2014). The grid was defined based on a mesh with 124 rows and 22 layers with cells of 85 × 12 m. It was refined near the FSI area (42 × 12 m) and surface area (42 × 6 m). These dimensions of the model were applied to the case study model and for the sensitivity analysis. However, depth, topography, and basement were modified to test how the size of the model affects the temperature distribution. The flow was solved using the Pre-Conditioned Conjugate Gradient (PCG) solver. The solution method for the advective term of the transport equation was the Generalized Conjugate Gradient (GCG) solver with Jacobi pre-conditioner. The Courant number used was 0.75. The simulation of models 1 and 2 requires between 1000 and 1600 years to reach the steady-state conditions. However, simulation of the model 3 was run during 15 years.

For the boundary conditions, the basement of the aquifer and the left border were defined as a nonflow boundary (Neumann boundary condition). In the sea bed and right boundary, constant hydraulic heads and salinities were defined (Dirichlet boundary condition). With respect to the thermal boundary conditions, temperature recorded data from W180 were used to establish them; on the other hand, temperature measurements of W60, W250, and W10 were used to calibrate the study model.

The workflow with the numerical models included a sensitivity analysis and a real case simulation. Sensitivity analysis was conducted to assess the effect of model parameters on heat transport in coastal aquifers. To reproduce the field observations with the real case study model, specific site characteristics, obtained from previous studies (Duque et al., 2008; Duque et al., 2018; Sánchez-Úbeda et al., 2018a) and fieldwork, were considered, such as aquifer geometry, hydraulic conductivity, heterogeneity, and hydraulic gradient. In the process, three different models (Models 1, 2, and 3) were constructed addressing the different purposes, and the boundary conditions were modified for each of them (Fig. 4 and Table 1):

4. Results

4.1. Temperature distribution

An initial synthetic cross section of the temperature distribution of a coastal aquifer was obtained based on model 2, which was compared with model 1 (Fig. 5). The hydraulic conductivity used was Kx = 1 and the anisotropic ratio Kx/Kz = 10, and the boundary conditions and the rest of the input parameters are specified in Fig. 4 and Table 1. Groundwater temperature increases with depth due to the geothermal gradient. However, temperature propagation and thermal contours are bent because of the change in flow direction (Fig. 5a), generating a hotter temperature plume along the FSI. At deeper locations in the aquifer, fresh groundwater is forced to ascend toward the sea due to the presence of the salt wedge, which implies greater heat transport than other parts of the aquifer where convection is less important. In turn, temperature also affects the position of the FSI. When adding temperature to the model (comparing model 1 and model 2), the FSI width changed, but it also rotated and moved its toe inland (Fig. 5b). The FSI toe moved tens of meters when temperature difference between the surface and basement is 1 °C for our case study; however, it is also highly

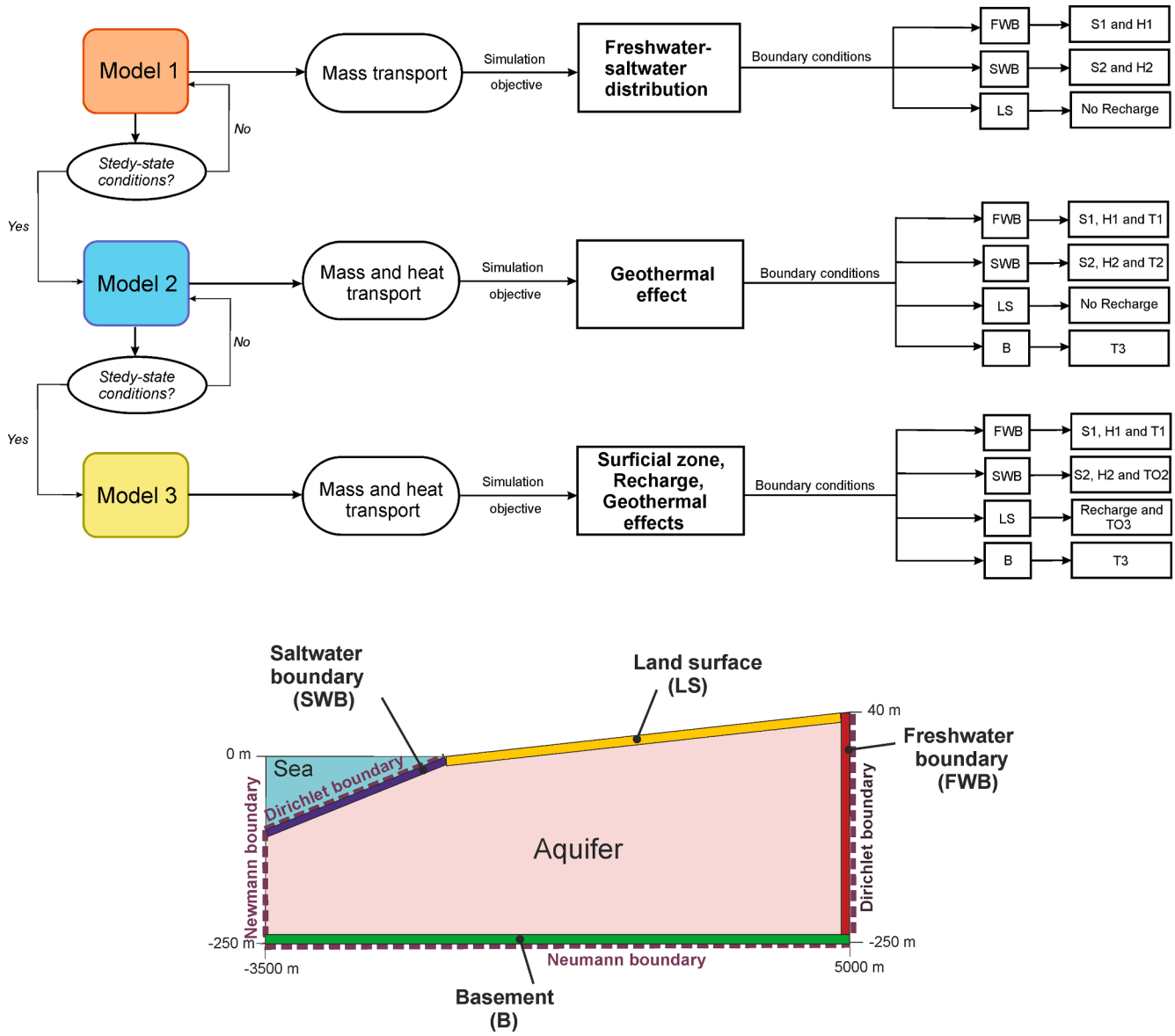

Fig. 4. Steps of the simulation and boundary conditions of the numerical model. The values of salinity, hydraulic head and temperature are specified in Table 1.FWB: Freshwater boundary, SWB: Saltwater boundary, LS: Land surface, B: Basement.

dependent on the aquifer properties. In general, an increase of temperature difference will favor the encroachment of seawater. This is consistent with Henry and Kohout (1972) and Langevin et al. (2010), who indicated that convective cells are stronger when density is affected by temperature. Groundwater is heated at the bottom of the aquifer, rises because of the combination of the effect of the saline wedge and the buoyancy effect in warmer water, and saltwater replaces the heated upward water.

4.2. Sensitivity analysis

Heat transport is controlled by different parameters: hydraulic conductivity, porosity, dispersivity, thermal distribution coefficient, thermal diffusivity, hydraulic gradient, thermal boundary, seafloor slope, and depth of the basement. Sensitivity analysis of the variable-density groundwater flow and heat transport model showed the impact of each parameter on thermal distribution. The sensitivity analysis was focused on heat transport within the deep zone of each model and especially around the area of the FSI. Thus, modeling of this section consisted of a variable-density model with geothermal heat input (Fig. 4). The value of the parameters was changed for a range based on realistic values obtained in the literature (specified in Table 1). The assignation of maximum, mean, and minimum values to each parameter aimed to cover those parameters with scarce information and to show the differences associated with the natural variability in aquifers. Homogeneous conditions were assumed with a hydraulic conductivity of Kx = 1 m/d, a Kx/Kz ratio of 10, and the input parameter values of Table 1, except for the parameter that was tested in each case.

4.2.1. Hydraulic conductivity

Four sets of hydraulic conductivities were tested obtained from the literature (Calvache et al., 2009; Duque et al., 2017): two with a lower hydraulic conductivity (Kx = 1 m/d and changing anisotropic ratios Kx/Kz of 1 and 10) and two with higher hydraulic conductivity (Kx = 300 m/d and anisotropic ratios Kx/Kz of 1 and 10). The resulting temperature distribution of the different scenarios showed changes in the order of magnitude of hundreds of meters, depending on the value of the hydraulic conductivity (Fig. 6). Lower hydraulic conductivity generated thermal contours distributed parallel to the base of the aquifer, while higher values related to more changes in the section. Anisotropy played

Table 1
Input values of the parameters for the sensitivity analysis and study model.

Input parameters	Sensitivity analysis	Case study model	Source
Specific storage	1E-5 m^{-1}	1E-5 m^{-1}	Calvache et al. (2015)
Specific yield	0.25	0.25	Similar value to Calvache et al. (2009)
Porosity θ	0.2–0.6	0.3	Duque et al. (2008)
Longitudinal dispersivity	1–100 m	10 m	Sauffer et al. (2013)
Horizontal transverse dispersivity	0.5–50 m	5 m	Sauffer et al. (2013)
Vertical transverse dispersivity	0.5–50 m	5 m	Sauffer et al. (2013)
Freshwater salinityS_1	350 mg/L	350 mg/L	Field observations
Saltwater salinity S_2	35000 mg/L	35000 mg/L	Field observations
Freshwater boundary head H_1	15–35 m	17 m	Field observations
Saltwater boundary headH_2	0 m	0 m	Field observations
Freshwater temperature T_1	17.2 °C	16.7 °C	Field observations
Saltwater temperature T_2	13 °C	16.7 °C	Manca et al. (2004)
Basement temperature T_3	19–30 °C	20.05 °C	Field observations
River water temperature oscillation TO_1	–	Sinus function 12–26 °C	Based on Duque et al. (2010)
Seawater temperature oscillation TO_2	–	Sinus function 14–24 °C	State of Harbors (Spanish Ministry)
Molecular diffusion coefficient D_m^s	1E-10 m^2/d	1E-10 m^2/d	Langevin et al. (2007)
Thermal conductivity of waterk_{Tfluid}	0.58 W/m°K	0.58 W/m°K	Langevin et al. (2007)
Thermal conductivity of sediments k_{Tsolid}	1–6 W/m°K	2.9 W/m°K	Approximate value for gravel (Xiaoqing et al., 2018)
Specific heat of water C_{Pfluid}	4186 J/kg°K	4186 J/kg°K	Langevin et al. (2007)
Specific heat of sediments C_{Psolid}	100–1000 J/kg°K	830 J/kg°K	Approximate value for gravel (Xiaoqing et al., 2018)
Thermal diffusivity D_m^T	0.06–0.3 m^2/d	0.15 m^2/d	Calculated using eq. (4)
Bulk thermal conductivity k_{Tbulk}	0.87–4.37 W/m°K	1.8 W/m°K	Calculated using eq. (5)
Thermal distribution factor K_d^t	2E-8 – 2E-7 L/mg	2E-7 L/mg	Calculated using eq. (3)
Density change with concentration	0.7	0.7	Langevin et al. (2007)
Density change with temperature	−0.375 kg/(m^3 °C)	−0.375 kg/(m^3 °C)	Langevin et al. (2007)
Density vs pressure head slope	0.00446 kg/m^4	0.00446 kg/m^4	Langevin et al. (2007)
Bulk density ρ_b	1800 kg/m^3	1800 kg/m^3	Calculated with $\rho_b = \rho_s(1-\theta)$
Reference temperature	25 °C	25 °C	Langevin et al. (2007)
Viscosity vs concentration slope	1.923E-6 m^4/d	1.923E-6 m^4/d	Langevin et al. (2007)
Reference viscosity	86.4 kg/ m d	86.4 kg/ m d	Langevin et al. (2007)

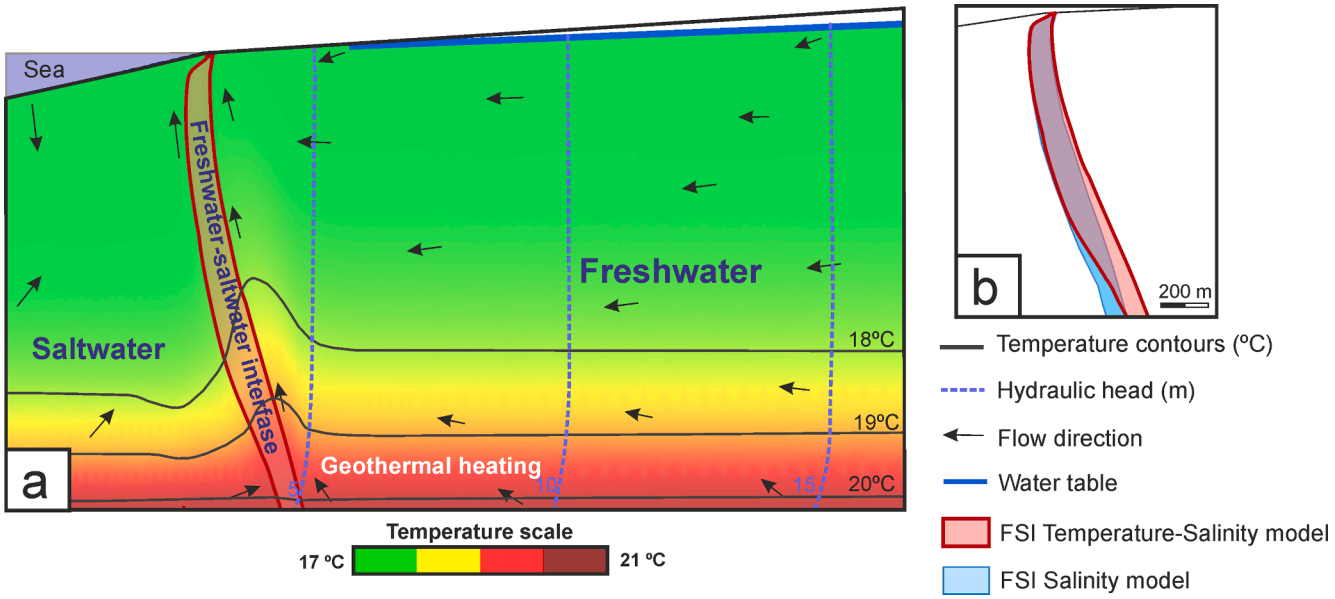

Fig. 5. A. Synthetic cross section of the temperature distribution of a coastal aquifer. B. Freshwater-saltwater interface (FSI) position simulated with a variable-density mass transport model with and without temperature.

a more important role in the area where the flow components were more vertical; that is, along the zone where the FSI is located. High hydraulic conductivities (300 m/d) produced a sharper rise in the thermal plume than low hydraulic conductivities (1 m/d).

Anisotropy of Kx/Kz = 10 generated a higher horizontal than vertical component, hindering vertical heat transport and flattening the thermal contours. Anisotropy favored the horizontal flow thereby displacing the FSI seawards, and the thermal plume was affected in the same manner due to the direct relationship with the FSI. This test indicates that the anisotropy can cause a change on an order of magnitude of tens of meters in the thermal distribution under the boundary conditions selected.

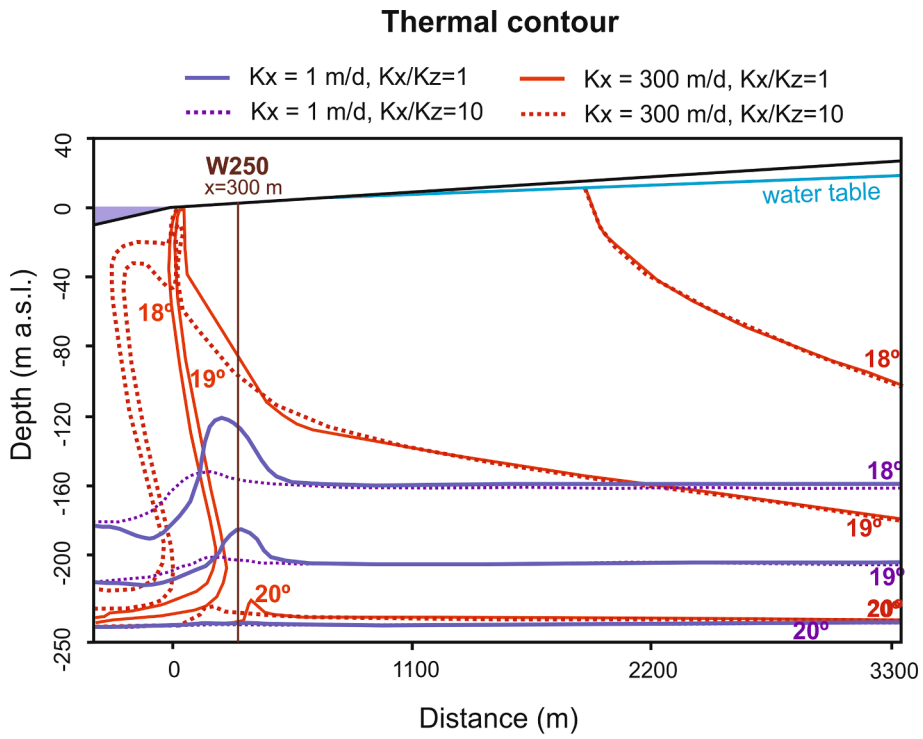

Fig. 6. Thermal contours distribution resulting from models with different values of hydraulic conductivity.

4.2.2. Porosity (θ)

The sensitivity of temperature to porosity was evaluated by introducing two extreme values (0.2 and 0.6) to the model obtained from the literature (Freeze and Cherry, 1979). Although the depth of the thermal contours was very similar for both cases, there were slight differences in the shape of the isothermal lines (Fig. 7a). For $\theta = 0.6$, the thermal contours became flattened and therefore, the geothermal gradient was practically the same for any observation point on the x-axis. For $\theta = 0.2$, the thermal plume was slightly higher. Likewise, the FSI varied depending on the porosity value. For $\theta = 0.6$, the FSI was narrower in the upper area in comparison with a $\theta = 0.2$.

This indicates that a reduction in porosity is related to higher advective transport; hence, the buoyancy effect is larger, which causes a modification in the upper part of the FSI (fresh groundwater discharge zone) and, consequently, in the temperature distribution. Nevertheless, the effect of this parameter is very reduced considering the range of values tested. For the range of porosities commonly found in real aquifers, the differences would be minor.

4.2.3. Dispersivity (α)

Both salinity dispersivity and thermal dispersivity were considered, as they are modeled in an analogous manner (deMarsily, 1986); therefore, they have the same value (Bridger and Allen, 2010; Engelhardt et al., 2013). The thermal dispersivity of aquifers usually ranges from 0.1 to 100 m (Stauffer et al., 2014). The three values for the dispersivity tensor (α) were considered based on the dimensions of the model (1 m, 50 m, and 100 m). The temperature profiles obtained 300 m from the coastline showed that higher dispersivity ($\alpha = 100$ m) increased temperature throughout the entire thickness of the aquifer (Fig. 7b), as the heat effect from the geothermal source of heat can spread more easily. For $\alpha = 1$ m, the trend of the temperature profile was more concave, whereas temperature increased more linearly with depth for $\alpha = 100$ m. When thermal dispersivity played a more important role in heat transport, heat convection decreased. Hence, weaker convection (and thus dispersivity-dominant heat transfer) produced a linear increase in temperature, as demonstrated by An et al. (2015).

The temperature difference reached more than 1 °C, which had significant relevance in the comparison with other parameters. A dispersivity of approximately 100 can move water with a temperature of 18 °C upwards to the shallow part of the aquifer. This has not been possible to reach with the sensitivity analysis of the other parameters.

4.2.4. Thermal distribution coefficient (K_d^t)

K_d^t was estimated with equation (3) applying maximum, minimum, and mean values of C_{Psolid} for rocks and minerals reported in the literature (Schärli and Rybach, 2001; Clauser, 2011). The resulting values of K_d^t were 2.3×10^{-7}, 1.27×10^{-7} and 2.3×10^{-8} L/mg. The sensitivity analysis showed variations up to tens of meters in the distance from the basement to the thermal contours D(B, tc_i) (Fig. 8a): a low value of K_d^t (2.3×10^{-8} L/mg) generated a greater D(B, tc_i), i.e., a further propagation of the thermal signal compared with higher values of K_d^t. The shallowest thermal contour (18 °C) was the one with greater displacement from the basement when changing the values of K_d^t. These results are consistent with the fact that K_d^t works as a retardation coefficient that causes the temperature changes to be slower than the linear flow velocity (Langevin et al., 2008). If more heat is necessary to increase the sediment temperature, the retardation of heat transport will increase (Ma et al., 2012). K_d^t had no direct effect on the salinity distribution but did on the heat distribution; therefore, the FSI can be affected by the buoyancy effect. However, the changes were so small that they were not appreciable in these simulations.

4.2.5. Thermal diffusivity (D_m^T)

The thermal diffusivity D_m^T was calculated with equations (4) and (5) using the given value of k_{Tsolid}. The maximum and minimum values and a middle value of k_{Tsolid} were estimated for different lithologies and were obtained from Xiaoqing et al. (2018). The values assigned to D_m^T were 0.3, 0.15, and 0.06 m^2/d, corresponding to dolomites, marlstone, and mudstones, respectively. The results of each simulation were observed in different locations of the model and represented with the R parameter (Fig. 8b).

Modification of the values of D_m^T produced a greater variability in R for the thermal contour of 18 °C. In contrast, R did not change for the

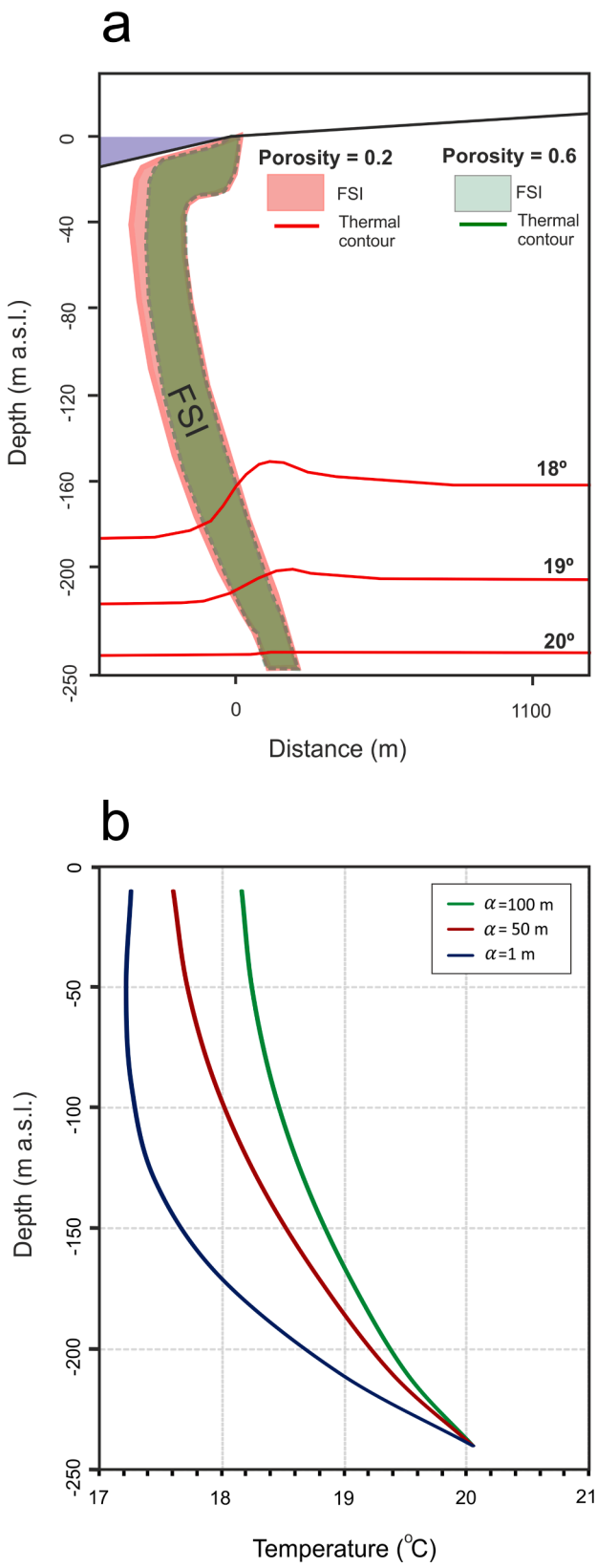

Fig. 7.a. a. Position of the FSI and the thermal contours resulting from models with different values of porosity. b. Temperature profiles at x = 300 m (W250 location) obtained for different values of dispersivity.

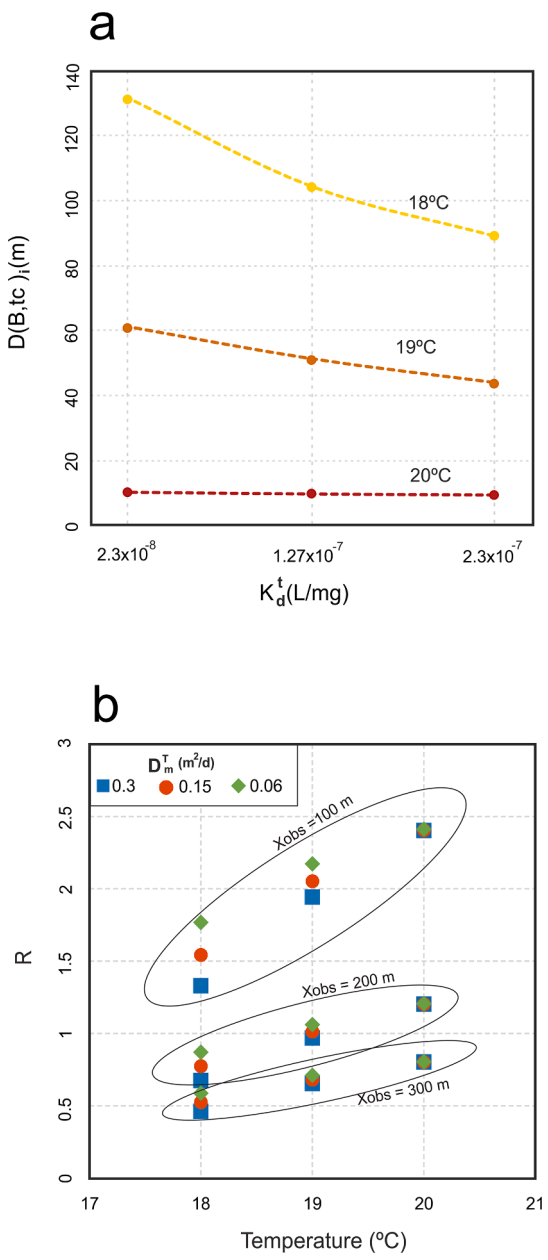

Fig. 8. a. Model results for different values of thermal distribution coefficient (K_d^t) obtained at x = 300 m (W250 location). b. Model results represented by R vs temperature of the thermal contours for different values of thermal diffusivity (D_m^T).

thermal contour of 20 °C when changing D_m^T. For $D_m^T = 0.06$, the R value can reach 24 % higher than that for $D_m^T = 0.3$, as is the case of the thermal contour of 18 °C observed at $X_{obs} = 100$ m. Just as K_d^t, the thermal contour of 18 °C showed larger changes than the rest of the temperatures due to the greater vertical component of the flow at this depth. The variation in the FSI position was so small that it could not be detected while testing the different values of D_m^T.

4.2.6. *Hydraulic gradient (Δh)*

The hydraulic gradient in aquifers is a variable parameter in time and space. Seasonal oscillation in recharge conditions can modify it in short periods. The impact on heat transfer was tested with a range between 0.003 and 0.007 from the lateral inflow. The constant head of the sea boundary was maintained at 0, and only the constant head of the freshwater boundary was changed (from 15 m to 35 m). These changes

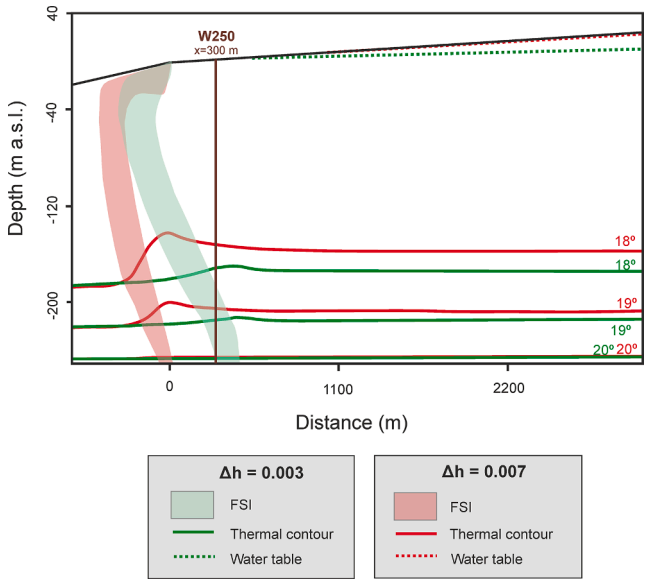

Fig. 9. Comparison of the thermal contours distribution and FSI position for two different hydraulic gradients.

were on the same order of magnitude as observed in the Motril-Salobreña aquifer during the last 20 years (Duque et al., 2010). Δh changed the distribution of salinity moving the FSI hundreds of meters and temperature by changing the pattern (Fig. 9). For Δh = 0.007, the FSI was positioned more seaward and vertical, and the temperature transport had a higher vertical component throughout the entire model compared with the results for Δh = 0.003. Additionally, the thermal plume in the discharge zone moved seaward and had a more pointy shape.

4.2.7. *Thermal boundary*

The effect of the input of geothermal heat was tested based on different rates. As the geothermal gradient increased 1 °C per 20 to 40 m of depth (Anderson, 2005), and the model was 250 m deep, the highest temperature difference between the surface and basement (ΔT) was 13 °C. Additionally, a ΔT of 6 °C and 2 °C were also tested. As the shallow part of the aquifer was assigned 17.2 °C, the basement of the model was 30 °C, 23 °C, and 19 °C. The ΔT was compared with the temperature distribution at different depths (-30 m, −100 m, −160 m, and −230 m) at × = 300 m (Fig. 10a). The point where the resultant lines intersected the x-axis, represented the temperature of a homoeothermic aquifer in which temperature would be homogeneous regardless of depth. ΔT = 13 °C produced an increase in temperature in the shallowest observation point (-30 m) of 3 °C with respect to the homoeothermic aquifer. There were small changes in the FSI position: for higher ΔT, the FSI had more verticality (a few meters seaward of the FSI toe) and was wider than for smaller ΔT, although there were no large differences.

4.2.8. *Seafloor slope (SFS)*

The seafloor geometry of the model was tested in order to study its relevance on temperature distribution. The different slope values used were: 2.8 % based on the estimated value for the Motril-Salobreña aquifer by bathymetric techniques (Jabaloy-Sánchez et al., 2014) and a minimum and maximum values of 0% and 5% respectively, to take account of other possible SFS representative of more study areas (Fig. 10b). The starting point of the slope was the coastline, and the continental topography was not changed regarding previous models. For SFS = 5%, the thermal contour had a larger *R* parameter in comparison with the rest of the inclinations, which indicates that the isotherms ascended less. For SFS = 5% the R value can reach 9% higher than that for SFS = 0%, as is the case of the thermal contour of 18 °C observed at

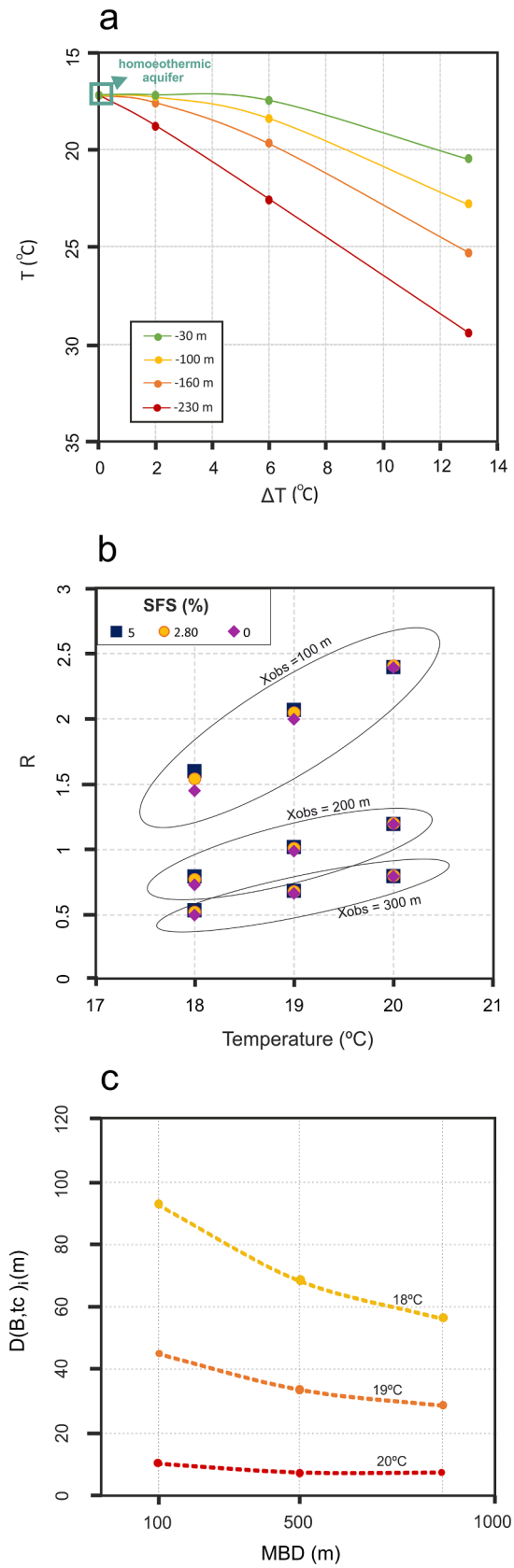

Fig. 10. a. Temperature variation by adding different geothermal inputs at different depths for three different values of geothermal gradients. Obtained at x = 300 m. b. Model results represented by R vs temperature of the thermal contours for different seafloor slopes. c, Distance of each thermal contour to the basement in different depth models.

X_{obs} = 100 m. The thermal contour of 18 °C, as it was located at a shallower location in the aquifer, was more affected by the change in slope than the other isotherms, and this sector had greater vertical flow components. Thus, the higher the seafloor slope is, the lower the elevation of the thermal contour. Moreover, the slope of the seafloor had an impact on the position of the FSI. For SFS = 5%, the FSI is less vertical, and its toe is situated a few meters seaward than for SFS = 0%.

4.2.9. Model basement depth (MBD)

Three model basement depths (MBD): 100 m, 500 m, and 1000 m, were considered (Fig. 10c). Although an increase in depth is usually associated with a major geothermal gradient, the temperature of the basement boundary was the same for all cases since the target was to understand their influence separately. The results showed important variations in the distance from the basement to the thermal contours D (B, tc_i); for example for D(B, $tc_{18°C}$), the difference between a model of 100 and 1000 m was almost 40 m.

4.3. Case study model

The model had the same structure as the model used for sensitivity analysis but the parameters were adjusted based on the local knowledge of the areas (Table 1). Horizontal layers without lateral facies changes were defined as this is the major sedimentary architecture of the aquifer. Smaller scale heterogeneity was not introduced to focus on major aspects of the thermal distribution.

Hydraulic conductivity was initially defined based on previous studies (Calvache et al., 2009; Duque et al., 2018) and the lithological core of W250 (Fig. 1). Model results were compared with the field measurements of temperature and salinity in W10, W250, and W60.

For temperature boundary conditions, a fixed temperature (20.05 °C) was assigned to the base of the aquifer based on the expected temperature at −250 m due to the linear temperature increment in W180 (Fig. 2). Temperature of the right boundary (freshwater entry) was 16.7 °C, which is an approximate value for temperature in the intermediate zone. The temperature oscillation assigned to the seafloor fluctuated between 14 and 24 °C. At the surface boundary, a constant recharge of 5000 mm/yr was assigned that represented the river inflow to the aquifer, as the observation wells were all located at a maximum distance of a few tens of meters from the trace of the river. The temperature of this recharge was a sinus function according to the seasonal oscillation of the river water temperature: 12–26 °C (Duque et al., 2010). In the calibration, hydraulic conductivity of the different layers was adjusted as well as temperature in the right boundary and in the recharge. These changes were minor adjustments, as still the boundary conditions were coherent with the field measurements (i.e., temperature value of the right boundary was modified to 16.7 °C, from 17.2 °C). Additionally, the adjusted recharge was four times smaller than that estimated in previous studies. The model was run for a total of 15 years to give enough time to reach the semistability, which was reached in the 9th year of simulation. From this time, the FSI position and geothermal heat were in steady state, and the temperature of the surficial zone and saltwater had repeated seasonal oscillations annually. The results displayed below correspond once the steady-state condition had been reached.

The coefficient of determination (R^2) of the calculated rating curves was 0.81, and the RMSE was 0.37 °C.

The vertical profiles of temperature at x = 300 m are displayed with the field data obtained from W250 (Fig. 11A). The differences in the first few meters correspond with the seasonal temperature oscillation. From −50 m, these differences were buffered, indicating that recharge had no influence. However, in the field data, temporal variations were observed when W250 intersected the FSI (from −150 m). This issue is discussed in

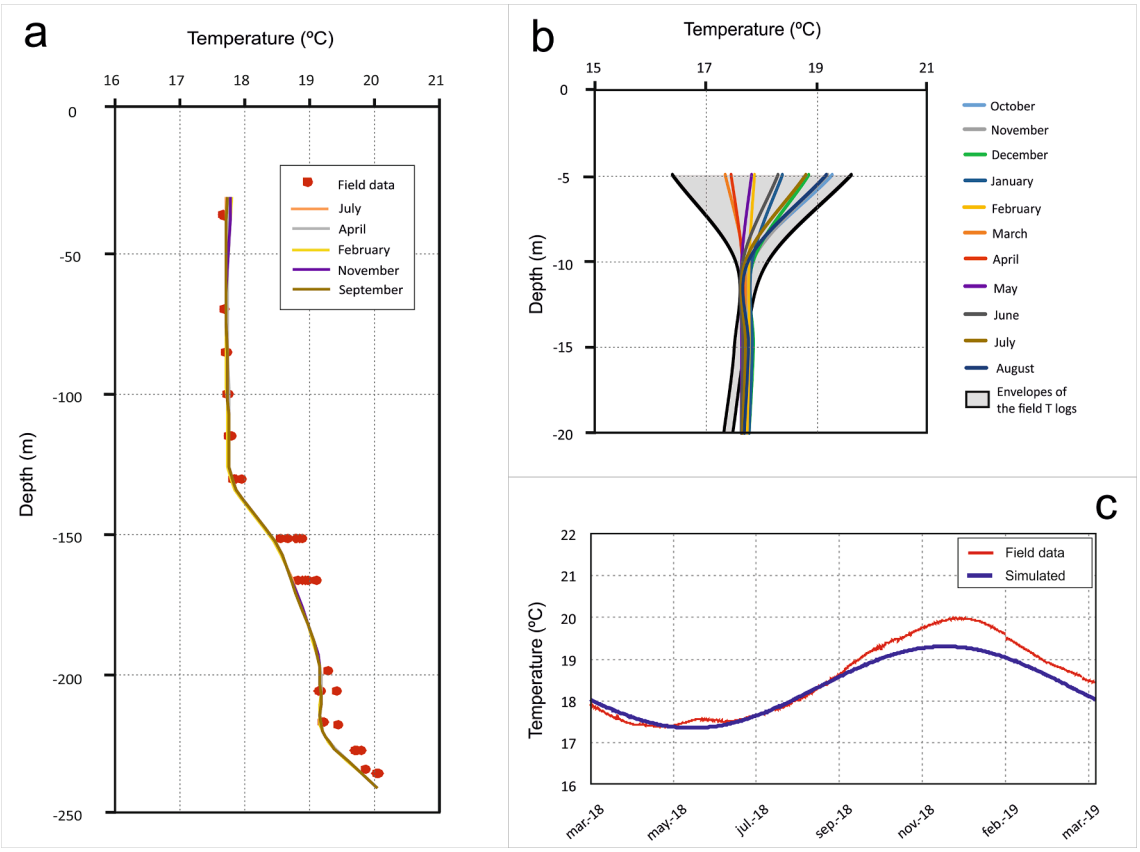

Fig. 11. Temperature results once the model reached the semisteady state: model simulation vs field data. 11a: Deep temperature logs at W250. 11b: Shallow temperature logs at W60. 11c: Seasonal oscillation in the surficial zone obtained at W10.

Table 2
Hydraulic conductivity values defined in each layer of the study model.

	Thickness (m)	Hydraulic conductivity (m/d)
Layer 1	16	Kx = Ky = 5 and Kz = 0.5
Layer 2	121	Kx = Ky = 400 and Kz = 40
Layer 3	63	Kx = Ky = 30 and Kz = 5
Layer 4	12	Kx = Ky = 150 and Kz = 1
Layer 5	35	Kx = Ky = 20 and Kz = 2

the next section. There is a strong connection between hydraulic conductivity values of the model (Table 2) and temperature distribution. The intermediate zone of the temperature profiles was related to a layer with high hydraulic conductivity (layer 2). This suggested that the temperature distribution is strongly dependent on the geology of the study area. The seasonal temperature oscillation in the surficial part of the aquifer was analyzed by the temperature logs at x = 700 m (Fig. 11B) and compared with the envelopes of the field logs measured in W60. The results ranged between 17.3 and 19.1 °C and were between the maximum and minimum envelopes (16.4–19.6 °C) and had very similar shapes. The profile with the minimum value was slightly lower than the minimum field measurement.

The thermal signal obtained at −5 m at x = 285 m demonstrated that the model was able to simulate seasonal oscillations (Fig. 11C). The sensor installed in W10 showed temperature oscillations with a maximum of 20 °C in December and a minimum of 17.5 °C in May, and the simulated temperature oscillated from 17.3 to 19.3 °C; therefore, the maximum value was slightly lower than the observed value.

For temperature distribution near the sea boundary, the simulated data obtained at x = -600 m (Fig. 12a) reflected the relevance of sea temperature to groundwater temperature in the saltwater domain. Groundwater under the sea followed the seasonal oscillation of sea temperature, but the amplitude was smaller and the delay increased with depth. At z = -50 m, oscillation could be observed, although the signal was poor. Cross sections of temperature distribution (Fig. 12b and 12c) showed that, below the surficial zone, the temperature of the freshwater domain was maintained at approximately 17 °C during summer and winter. This means that FSI acted as a barrier for temperature distribution because fresh groundwater removed the sea thermal signal due to the significant vertical flux near the discharge zone to the sea. In the vicinity of the FSI on the left side, there was a high infiltration of seawater. Consequently, the thermal signal was transferred to a greater depth, and a temperature mixing zone of several tens of meters was generated. This indicates the presence of an interface for temperature along the FSI that does not allow the heat transfer between freshwater and saltwater.

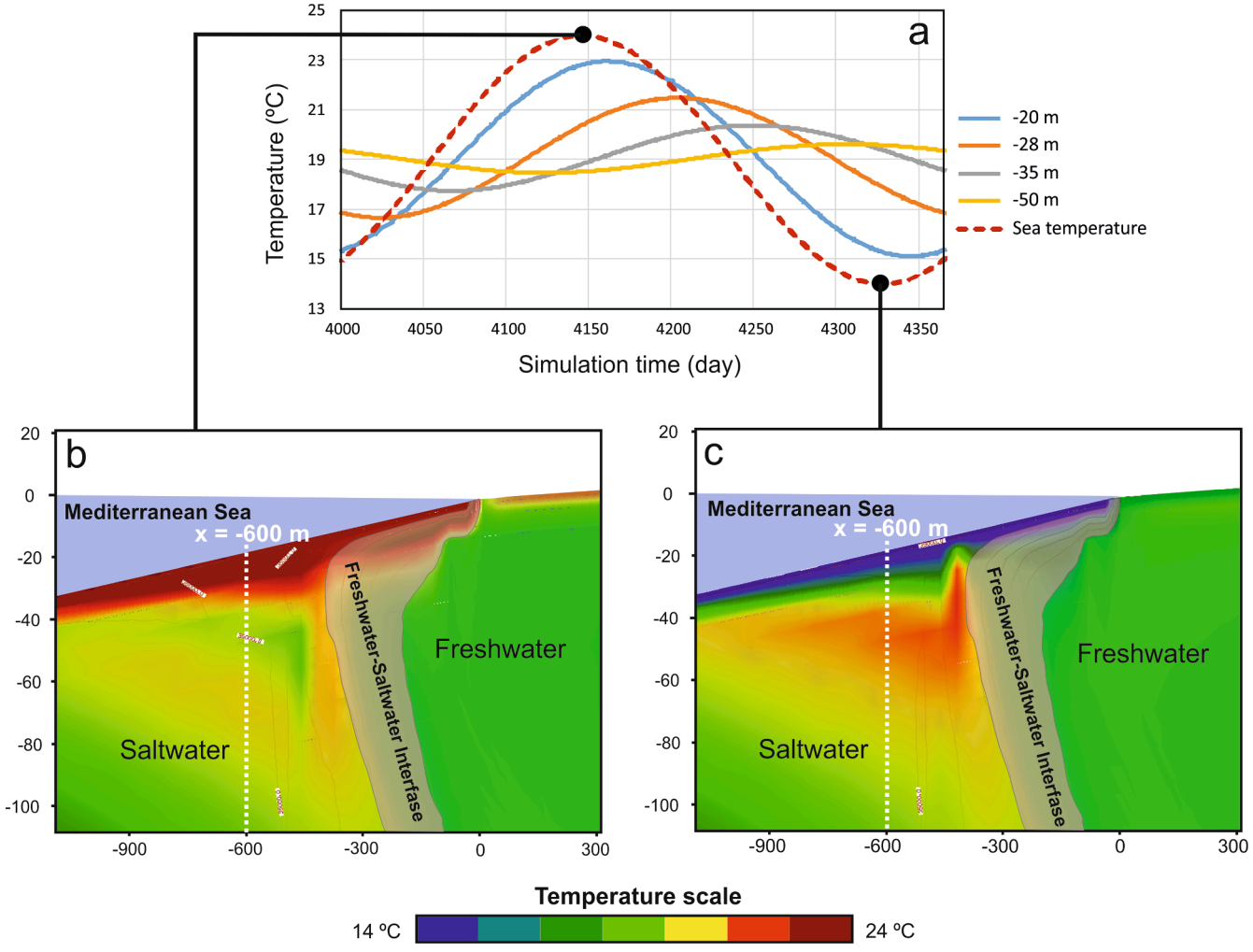

Fig. 12. Seawater temperature signal obtained by the study model. 12a: Time series at different depths at x = -600 m. 12b: Vertical section when the sea had the maximum temperature. 12c: Cross section when the sea had the minimum temperature.

5. Discussion

Sources of different temperatures and hydrodynamics established in coastal aquifers, including variable-density convective processes, generate a challenging scenario for developing temperature models. The availability of temperature data is scarce, as this parameter has not traditionally garnered extensive attention, but also because of the lack of deep wells in the proximity of the sea due to the dearth of salty water utilization.

The development of a numerical model improved the knowledge of temperature distribution within coastal aquifers and the generation of a prototype compiling the main characteristics of these areas regarding temperature and the interaction with variable density. Preliminary simulations disclosed the existence of thermal warm upwelling below the discharge area. An et al. (2015) and Szijártó et al. (2019) simulated this phenomenon with a groundwater flow model but in a freshwater setting, where flow moved upwards in discharge areas; however, coastal areas and variable density were not considered. There was a lack of information about temperature distribution in coastal aquifers and the differences with other types of groundwater systems, such as the dependence of the warm plume on the position and shape of the FSI. Additionally, the FSI changes because of the buoyancy caused by temperature over density of water, which is consistent with the convective cells demonstrated in a laboratory experiment (Henry and Kohout, 1972) and in a small dimensional model (Langevin et al., 2010) based on a previous experiment. Environmental tracers also indicated the rise of old deep groundwater nearby the FSI (i.e. Sánchez-Úbeda et al., 2018b; Calvache et al., 2020), indicating that the temperature distribution in coastal aquifers could be directly related to the age distribution.

Sensitivity analysis allowed us to quantify the order of magnitude of the impacts of the different parameters that are used for simulating temperature in coastal aquifers. These results are based on an aquifer that has been used as a reference (the Motril-Salobreña aquifer) and the implementation of much higher and lower values in the range of what can be

considered common in natural settings (see section 4.2.). Therefore, the impact of each value Table 3. can be used as a general indicator but in settings that differ extremely from our starting point (for example, karstified, highly heterogeneous, or extreme in size aquifers- i.e., a few meters deep aquifer) which should be used more carefully.

K is the most controlling parameter in the temperature distribution of a coastal aquifer. This can be applied to noncoastal aquifers (Ma et al., 2012; An et al., 2015). The Kx/Kz ratio had a notable influence on the vertical component of heat transport. The importance of this parameter increased in coastal areas due to its impact on the position of the FSI, on which heat transport depends. Both of them must be considered the primary calibration parameters when modeling a coastal aquifer.

Heat distribution of the entire aquifer is influenced by the temperature established at the base of the model, which is associated with geothermal heat. Thus, ΔT should be treated with special attention in studies based on aquifers located in zones with positive anomalies in the geothermal gradient, such as tectonically and volcanically active zones (geothermal gradients greater than 40 °C/km), as well as thin aquifers. Additionally, even thick aquifers with normal geothermal gradients (30 °C/km) can have relatively high temperatures, such as the southern Permian Basin in Europe (Limberger et al., 2018).

There are conflicting points of view in the literature about the role of dispersivity in heat transport. Some authors (i.e., Bear, 1972; Ingebritsen and Sanford, 1998; Hopmans et al., 2002) have given greater weight to conduction and have ignored thermal dispersivity. While others (i.e., Molina-Giraldo et al., 2011; Park et al., 2015; Piga et al., 2017) have given a higher relevance to thermal dispersion in their studies. Our research showed how dissipation of heat energy leading to high dispersivity values in a coastal aquifer could change the temperature pattern.

An aquifer with a deeper basement kept the thermal contours closest to the bottom compared with a model with a small MBD and the same boundary conditions. Reduction in heat transport at a greater MBD is related to the findings of Szijártó et al. (2019), who suggested that flux decreased with the increase in deeper models.

Both K_d^t and D_m^T were the least sensitive parameters for temperature modeling in a previous study using a heat tracer test (Ma et al., 2012). However, our results showed that larger values of K_d^t and D_m^T maintained the temperature input generated by geothermal heat near the basement, preventing the ascent of thermal contours. This is because the heat is dispersed quickly and cannot ascend to the upper layers of the aquifer.K_d^t and D_m^T depend on C_{Psolid} and k_{Tsolid} respectively; therefore, aquifer materials play an important role in conduction transfer when they reach higher values of K_d^t and D_m^T.

The effect of hydraulic gradient has a direct impact on the position of the FSI and hence the thermal plume. The same happened with the increase in hydraulic conductivity, although the magnitude of heat propagation was considerably lower for the hydraulic gradient. For this reason, Δh could play a more relevant role in areas with climatic variability (strong seasonality) where hydraulic heads will vary due to changes in recharge.

Geometry of the seafloor and its impact on the FSI has been previously studied, and a bigger SFS led to an augmentation of the intrusion (Abarca et al., 2007; Walther et al., 2017). In our case, the range of values considered based on the studies in the area, do not have a significant effect compared with other parameters considered. The verticality of the FSI for smaller SFS also impacts on the temperature distribution in coastal aquifers because it favors the vertical component of the flux and the thermal contours were positioned more towards the surface.

Porosity was the least controlling parameter in the temperature distribution. It had an effect on both advection and convection components but in opposite ways (Panteli, 2018; Piga et al., 2017). An increase in porosity resulted in a decrease in the effective velocity of groundwater and a reduction in plume length but also caused a decrease in thermal conductivity (groundwater is less conductive than the solid phase), which increased plume length. The opposite effects compensated for each other; however, porosity slightly affected the advection component, and the plume was slightly larger at lower porosities. Ranjan et al. (2004) found that a change in porosity does not lead to a change in the position of the FSI, but only leads to a change in the length of time to achieve the steady state of the interface. However, our results showed that when heat transport is added to the model, porosity could affect the FSI by thermal buoyancy, though only slightly. Analysis of the changes in porosity is, in this case, a theoretical example because in real aquifers, changes in porosity, such as the extremes considered in this study, would likely be associated with changes in hydraulic conductivity that, as has been explained before, could have a strong impact on temperature distribution within the aquifer.

The study model of the Motril-Salobreña aquifer is the first attempt,

Table 3
Influence of each parameter or boundary condition on sensitivity analysis: variations on the distance between the basement and the thermal contour of 19 °C and in the position of the FSI toe.

Parameters	Variation of the D(B, $tc_{19°C}$)	Variation of the FSI toe position
Hydraulic conductivity	100's of meters	100's of meters
Thermal boundary	100's of meters	Few meters
Dispersivity	Several 10's of meters	100's meters
Model basement depth	Several 10's of meters	1000's meters
Thermal distribution coefficient	10's of meters	Few meters
Thermal diffusivity	10's of meters	Few meters
Hydraulic gradient	10's of meters	100's meters
Seafloor slope	Meters	Meters
Porosity	Few meters	Meters

to our knowledge, of a model including temperature and variable density that is calibrated based on field temperature data. It is a synthetic model of the natural system that consider recharge and the hydraulic gradient constant but with seasonal changes in temperature inputs. Although the results were consistent with observations, there are three aspects that should be clarified with this model. (1) Recharge was assigned continuously, but there were dry periods that could reduce the flow even if there was a dam that regulated river flow upstream. Additionally, recharge from the river to the aquifer was four times less than the recharge estimated in previous studies from the river to the aquifer (Calvache et al., 2009; Duque et al., 2011). However, this model does not simulate all river tracks over the aquifer, and infiltration is higher in the northern stretch of the river, which was not included in the model. (2) The hydraulic gradient has seasonal and interannual oscillations with dry and wet periods that in the model were represented with a mean value for both cases. (3) For the calibration of K, in line with the sedimentology in the study area (Fig. 1C), K was drastically reduced. The hydraulic conductivity value is due to the high topographic gradient (3482 m from the river head to the river mouth) that allows the deposition of coarse sediments. The geological and geometrical characteristics of the aquifer (depth, high K, and hydraulic gradient) are very relevant for the temperature pattern identified.

Comparison of the model results with the field observations showed some differences. The modeled temperature logs in W250 were constant over time (Fig. 11a); however, field measurements indicated slight variations at the depth where the FSI was intersected, i.e., at the intersection of the ascendant thermal plume. This contrasts with the field data in W180, where temporal variations were not observed (Fig. 2). This demonstrates that temperature in the proximity of the FSI was more exposed to changes related to variations in water entry to the aquifer, such as hydraulic gradient or surficial recharge. This hypothesis is reinforced by the sensitivity analysis (Fig. 9), indicating movement of the FSI on the order of magnitude of hundreds of meters and hence of the thermal plume due to changes in hydraulic gradient. Discrepancies between the model and field data regarding the movement of temperature are then due to the absence of changing recharge and hydraulic gradient in the model, and they can be the object of study in future research.

Oscillation of the recharge temperature allowed us to obtain a time series of temperature at x = 285 m (Fig. 11c) with better fitting than the vertical logs (Fig. 11b). Nevertheless, lateral changes in hydraulic conductivity would be needed to achieve a better calibration of the results. This model does not consider lateral changes in hydraulic conductivity that are likely to take place in the study area as it corresponds with a deltaic sedimentary architecture. However, it should be taken into consideration that there are field measurements that have been collected in different years and that climatic conditions are likely to be dissimilar. Therefore, both temperature data and model results must be considered general indicators of trends even if the results have achieved a very high degree of matching between observations and model results.

The recharge temperature was decided based on the average temperature of the air in this region. Nevertheless, for different seasons this temperature changes along the year with colder recharge during winter and warmer in summer. In this region, the temperature changes are relatively mild due to the proximity of the coast, also recharge is almost inexistent during the warmest months of the year. Still, a better characterization of recharge temperatures would be a useful input for further studies on this topic.

Changes in temperature generated by seawater infiltration are an infrequent parameter considered in previous studies. As hypothesized by Kohout (1965), seawater infiltrates the aquifer and is warmed by geothermal heating. However, he assumed a constant temperature. Our results demonstrated that seasonal oscillation of sea temperature created a thermal signal in the aquifer that only affected the saltwater domain. The FSI acts as a barrier for the thermal domains in freshwater, dominated by the temperature associated with the geothermal input and the temperature of the recharge and saltwater, affected by seawater infiltration and the deep processes associated with variable-density convection. Hydraulic conductivity and hydraulic gradient are clearly related favoring the flushing of the seawater thermal signal due to the upwards fresh groundwater flux near to the FSI. The thermal barrier could be sharper in the case of the Motril-Salobreña aquifer in comparison with other aquifers due to the relatively high hydraulic conductivity and hydraulic gradient. However, temperature separation is also expected in other study areas, although the thermal barrier would be more or less evident depending on the conditions of the area, such as the temperature difference between the aquifer and sea. Temperature variations along the sea water column were not considered in the model; instead, the same value of temperature was established at all depths. Preliminary analysis indicated that other parameters had more influence on the groundwater temperature distribution, however, its impact was not studied in detail due to the limited availability of seawater temperature data in depth. Cross-disciplinary collaboration with both oceanographic and hydrogeologic viewpoints would strengthen the perspectives on this matter as has been highlighted previously (Duque et al., 2020).

Human activities, such as pumping, altered groundwater flow producing saline upconing beneath the pumping area, and enhancing the seawater intrusion. The geometry of the FSI can be modified significantly with this process, as has been the case of the Andarax coastal aquifer (Stein et al., 2020). Given the close connection of the FSI with temperature distribution, human-induced changes can have a direct impact on the heat plume described in this work.

One general issue in the development of groundwater temperature models is how to obtain reliable temperature data. Temperature profiles inside wells can be highly affected by water circulation inside the casing, and even the mixing of water when collecting data can generate problems if this is not performed carefully. This problem has been discussed in previous research that has suggested alternative methods for measuring temperature, such as Shalev et al. (2009), Carrera et al. (2010), and Levanon et al. (2016). Some of the temperature data collected in this investigation have been obtained in similar wells, but systematic collection with monthly campaigns and continued activity for years indicates that the temperature profiles are consistent. For example, Elad et al. (2017) indicated how these types of measurements show significant trends and prevalent dynamics for salinity. It is not common to find deep wells in coastal areas well equipped for conducting research, and drilling prices are prohibitive; therefore, as long as drilling and measuring technology is in the current state, this type of temperature profile is our best approach for groundwater temperature research. A recent investigation using DTS fiber optic cables allowed us to obtain temperature profiles without flow inside the well (Folch et al., 2020), but still, the depth reached did not exceed 25 m. This also indicates the utility at the moment of the development of numerical models to further scientific knowledge in areas where it is challenging to collect high-quality data, such as sensitivity analysis conducted in this study. Further progress in the development of more realistic models, including lateral heterogeneity and seasonal hydrogeological processes, will contribute to a better knowledge of heat transport processes in coastal aquifers.

6. Conclusion

Heat sources for groundwater in coastal aquifers include surface water recharge, sea infiltration, and geothermal heat. Each source produces a thermal signal within the aquifer, generating changes in temperature at different depths. Recharge water temperature produces a surficial temperature zone that is highly variable throughout the year. Sea water temperature also produces a seasonal temperature oscillation within the saltwater domain. These two sources are affected by seasonal changes, while the Earth's internal heat induces a continuous geothermal gradient within the aquifer that increases with depth. In coastal aquifers, all these factors coalesce in the area where groundwater

discharges to the sea. Geothermal heat ascends, boosted by variable-density processes that bring deep aquifer water to the surface where recharge water and sea infiltration all meet, generating a complex mix of different temperatures.

The variable density and temperature transport model using SEAWAT revealed that the effect of the geothermal gradient is strongly dependent on the FSI and that the heat plume ascends following the FSI (i.e., thermal contour of 19 °C ascended 100 m in the proximity of the FSI for Kx = 300 m/d and Kx/Kz = 10). The shape and position of the thermal plume depend on different parameters, e.g. more flattened plumes affected by higher anisotropic ratios with the same values of Kx. In addition, temperature also influences water density; therefore, the FSI can be modified with respect to a model without temperature species. The FSI toe can be moved tens or even hundreds of meters depending on the aquifer properties by using or not using temperature.

The results indicated that the most sensitive parameters are hydraulic conductivity and thermal input at the base of the aquifer. These findings demonstrate the importance of convection on heat transport in an aquifer with these characteristics (high hydraulic conductivities and hydraulic gradient). The changes in parameters open a range of possibilities for research and work in this sector with a view on the application to other study areas.

The case study model integrates the three heat sources into the same model, which provides a better understanding of heat interactions with different origins, as there are no precedents on including all the different temperature sources in coastal aquifers. Furthermore, the model demonstrates the existence of a thermal barrier coinciding with the position of the FSI that separates the temperature of the saltwater and freshwater.

Despite our results are focused on one case study, many of our findings could be applied to other coastal aquifers as the temperature barrier of the FSI, the plume of higher temperature associated with geothermal heat, especially in aquifers with significant thickness, and the presence of different temperature sectors that can be identified at different depths. Still, geological conditions can play a fundamental role in these processes, and aquifers with higher heterogeneity, alternation of layers with high contrast in hydraulic conductivity or different temperature seasonality can generate a picture differing from what has been presented in this work. This is the first attempt at providing a full picture of temperature distribution in coastal aquifers but further research applying a similar methodology to other hydrogeological settings, climatic conditions, and with more focus on the simplified aspects that have been done in this study would help to provide answers to this emerging field of research. The use of heat as a tracer in hydrogeological studies is growing in interest, as this is a reliable and inexpensive tracer. In this study, we discussed the major processes and the effect of parameters on the application of temperature in coastal aquifers, where a number of processes generate a different picture of what can be found in other coastal or non-coastal settings.

CRediT authorship contribution statement

A.M. Blanco-Coronas: Conceptualization, Methodology, Software, Formal analysis, Data curation, Writing – original draft, Writing – review & editing, Visualization. **C. Duque:** Conceptualization, Methodology, Data curation, Writing – review & editing, Supervision. **M.L. Calvache:** Conceptualization, Resources, Data curation, Writing – review & editing, Supervision, Project administration, Funding acquisition. **M. López-Chicano:** Conceptualization, Resources, Data curation, Writing – review & editing, Supervision, Project administration, Funding acquisition.

Declaration of Competing Interest

The authors declare that they have no known competing financial interests or personal relationships that could have appeared to influence the work reported in this paper.

Acknowledgments

This study was supported by grant CGL2016-77503-R from the Ministry of Economy and Competitiveness (MINECO), cofounded by the European Regional Development Fund (ERDF) of the European Union (EU), and the RNM-369 research group of the regional government of Andalusia. The authors also thank the State Harbors (Ministry of Public Services, Government of Spain) for providing the sea temperature dataset. One of the authors conducted this work as part of the activities of the Aarhus University Centre for Water Technology, WATEC. Funding for open access charge: Universidad de Granada / CBUA.

References

Abarca, E., Carrera, J., Sánchez-Vila, X., Voss, C.I., 2007. Quasi-horizontal circulation cells in 3D seawater intrusion. J. Hydrol. 339, 118–129. https://doi.org/10.1016/j.jhydrol.2007.02.017.

An, Ran, Jiang, Xiao Wei, Wang, Jun Zhi, Li Wan, Xu, Wang, Sheng, Li, Hailong, 2015. Analyse Théorique de La Distribution de La Température de L'eau Souterraine à L'échelle D'un Bassin. Hydrogeol. J. 23, 397–404. https://doi.org/10.1007/s10040-014-1197-y.

Anderson, M.P., 2005. Heat as a ground water tracer. Groundwater. https://doi.org/10.1111/j.1745-6584.2005.00052.x.

Bakker, M., Caljé, R., Schaars, F., Van Der Made, K.J., De Haas, S., 2015. An active heat tracer experiment to determine groundwater velocities using fiber optic cables installed with direct push equipment. Water Resour. Res. 51, 2760–2772. https://doi.org/10.1002/2014WR016632.

Bear, J., 1972. Dynamics of Fluids in Porous Media. American Elsevier Publishing Company Inc., New York.

Befus, K.M., Cardenas, M.B., Erler, D.V., Santos, I.R., Eyre, B.D., 2013. Heat transport dynamics at a sandy intertidal zone. Water Resour. Res. 49, 3770–3786. https://doi.org/10.1002/wrcr.20325.

Bredehoeft, J.D., Papadopulos, I.S., 1965. Rates of vertical groundwater movement estimated from the Earth's thermal profile. Water Resour. Res. 1, 325–328.

Bridger, D.W., Allen, D.M., 2010. Heat transport simulations in a heterogeneous aquifer used for aquifer thermal energy storage (ATES). Can. Geotech. J. 47, 96–115. https://doi.org/10.1139/T09-078.

Calvache, M.L., Ibáñez, S., Duque, C., Martín-Rosales, W., López-Chicano, M., Rubio, J. C., González, A., Viseras, C., 2009. Numerical modelling of the potential effects of a dam on a coastal aquifer in S. Spain. Hydrol. Process. 23, 1268–1281. https://doi.org/10.1002/hyp.7234.

Calvache, M.L., Duque, C., Gomez Fontalva, J.M., Crespo, F., 2011. Processes affecting groundwater temperature patterns in a coastal aquifer. Int. J. Environ. Sci. Tech. 8, 223–236.

Calvache, M.L., Sánchez-Úbeda, J.P., Duque, C., López-Chicano, M., De La Torre, B., 2015. Evaluation of analytical methods to study aquifer properties with pumping tests in coastal aquifers with numerical modelling (Motril-salobreña aquifer). Water Resour. Manag. 30, 559–575. https://doi.org/10.1007/s11269-015-1177-6.

Calvache, M.L., Sánchez-Úbeda, J.P., Purtschert, R., López-Chicano, M.L., Martín-Montañés, C., Sültenfuβ, J., Blanco-Coronas, A.M., Duque, C., 2020. Characterization of the functioning of the Motril-Salobreña coastal aquifer (SE Spain) through the use of environmental tracers. Environ. Earth. Sci. 79, 141. https://doi.org/10.1007/s12665-020-8852-5.

Carrera, J., Hidalgo, J.J., Slooten, L.J., Vázquez-Suñé, E., 2010. Computational and conceptual issues in the calibration of seawater intrusion models. Hydrogeol. J. 18, 131–145. https://doi.org/10.1007/s10040-009-0524-1.

Clauser, C., 2011. Thermal Storage and Transport Properties of Rocks, I: Heat Capacity and Latent Heat. In: Gupta H.K. (eds) Encyclopedia of Solid Earth Geophysics. Encyclopedia of Earth Sciences Series. Springer, Dordrecht. 10.1007/978-90-481-8702-7_238.

Constantz, J., 1998. Interaction between Stream Temperature, Streamflow, and Groundwater Exchanges in Alpine Streams. Water Resour. Res. 34 (7), 1609–1615. https://doi.org/10.1029/98WR00998.

Dausman, A.M., Doherty, J., Langevin, C.D., Sukop, M.C., 2010. Quantifying data worth toward reducing predictive uncertainty. Groundwater 48, 729–740. https://doi.org/10.1111/j.1745-6584.2010.00679.x.

Debnath, P., Mukherjee, A., Singh, H.K., Mondal, S., 2005. Delineating seasonal porewater displacement on a tidal flat in the Bay of Bengal by thermal signature: Implications for submarine groundwater discharge. J. Hydrol. 529, 1185–1197. https://doi.org/10.1016/j.jhydrol.2015.09.029.

del Val, L., Carrera, J., Pool, M., Martínez, L., Casanovas, C., Bour, O., Folch, A., 2021. Heat dissipation test with fiber-optic distributed temperature sensing to estimate groundwater flux. Water Resour. Res. 57, 1–18. https://doi.org/10.1029/2020WR027228.

deMarsily, G., 1986. Quantitative Hydrogeology: Groundwater Hydrology for Engineers, 440 pp., Academic, Orlando, Fla.

Domenico, P.A., Palciauskas, V.V., 1973. Theoretical analysis of forced convective heat transfer in regional groundwater flow. GSA Bull. 84, 3803–3814. https://doi.org/10.1130/0016-7606(1973)84<3803:TAOFCH>2.0.CO;2.

Duque, C., Calvache, M.L., Pedrera, A., Martín-Rosales, W., López-Chicano, M., 2008. Combined time domain electromagnetic soundings and gravimetry to determine

marine intrusion in a detrital coastal aquifer (Southern Spain). J. Hydrol. 349, 536–547. https://doi.org/10.1016/j.jhydrol.2007.11.031.
Duque, C., Calvache, M.L., Engesgaard, P., 2010. Investigating river-aquifer relations using water temperature in an anthropized environment (Motril-Salobreña aquifer). J. Hydrol. 381, 121–133. https://doi.org/10.1016/j.jhydrol.2009.11.032.
Duque, C., López-Chicano, M., Calvache, M.L., Martín-Rosales, W., Gómez-Fontalva, J. M., Crespo, F., 2011. Recharge sources and hydrogeological effects of irrigation and an influent river identified by stable isotopes in the Motril-Salobreña aquifer (Southern Spain). Hydrol. Process. 25, 2261–2274. https://doi.org/10.1002/hyp.7990.
Duque, C., Muller, S., Sebok, E., Haider, K., Engesgaard, P., 2016. Estimating groundwater discharge to surface waters using heat as a tracer in low flux environments: The role of thermal conductivity. Hydrol. Process. 30, 383–395. https://doi.org/10.1002/hyp.10568.
Duque, C., Olsen, J.T., Sánchez-Úbeda, J.P., Calvache, M.L., 2018. Paleohydrogeological model of the groundwater salinity in the Motril-Salobreña aquifer. In: Calvache, M., Duque, C., Pulido-Velazquez, D. (Eds.), Groundwater and Global Change in the Western Mediterranean Area. Environmental Earth Sciences. Springer, Cham. https://doi.org/10.1007/978-3-319-69356-9_14.
Duque, C., Knee, K.L., Russoniello, C.J., Sherif, M., Abu Risha, U.A., Sturchio, N.C., Michael, H.A., 2019. Hydrogeological processes and near shore spatial variability of radium and radon isotopes for the characterization of submarine groundwater discharge. J. Hydrol. 579, 124192 https://doi.org/10.1016/j.jhydrol.2019.124192.
Duque, C., Michael, H.A., Wilson, A.M., 2020. The Subterranean Estuary: technical term, simple analogy, or source of confusion? Water Resour. Res. 56, 1–7. https://doi.org/10.1029/2019WR026554.
Eissa, M.A., de Dreuzy, J.R., Parker, B., 2018. Integrative management of saltwater intrusion in poorly-constrained semi-arid coastal aquifer at Ras El-Hekma, Northwestern Coast, Egypt. Groundw. Sustain. Dev. 6, 57–70. https://doi.org/10.1016/j.gsd.2017.10.002.
Elad, L., Yoseph, Y., Haim, G., Eyal, S., 2017. Tide-induced fluctuations of salinity and groundwater level in unconfined aquifers – Field measurements and numerical model. J. Hydrol. 551, 665–675. https://doi.org/10.1016/j.jhydrol.2016.12.045.
Engelhardt, I., Prommer, H., Moore, C., Schulz, M., Schüth, C., Ternes, T.A., 2013. Suitability of temperature, hydraulic heads, and acesulfame to quantify wastewater-related fluxes in the hyporheic and riparian zone. Water Resour. Res. 49, 426–440. https://doi.org/10.1029/2012WR012604.
Ferguson, G., 2007. Heterogeneity and thermal modeling of ground water. Ground Water 45, 485–490. https://doi.org/10.1111/j.1745-6584.2007.00323.x.
Folch, A., del Val, L., Luquot, L., Martínez-Pérez, L., Bellmunt, F., Le Lay, H., Rodellas, V., Ferrer, N., Palacios, A., Fernández, S., Marazuela, M.A., Diego-Feliu, M., Pool, M., Goyetche, T., Ledo, J., Pezard, P., Bour, O., Queralt, P., Marcuello, A., Garcia-Orellana, J., Saaltink, M.W., Vázquez-Suñé, E., Carrera, J., 2020. Combining fiber optic DTS, cross-hole ERT and time-lapse induction logging to characterize and monitor a coastal aquifer. J. Hydrol. 588, 125050 https://doi.org/10.1016/j.jhydrol.2020.125050.
Forster, C., Smith, L., 1989. The influence of groundwater flow on thermal regimes in mountainous terrain: A model study. J. Geophys. Res. 94, 9439–9451. https://doi.org/10.1029/JB094iB07p09439.
Freeze, R.A., Cherry, J.A., 1979. Groundwater. Prentice-Hall. Inc., Englewood Cliffs, N.J.
Glover, R.E., 1959. The pattern of fresh-water flow in a coastal aquifer. J. Geophys. Res. 64, 457–459. https://doi.org/10.1029/JZ064i004p00457.
Harbaugh, A.W., Banta, E.R., Hill, M.C., Mcdonald, M.G., 2000. MODFLOW-2000, The U. S. Geological Survey modular ground-water model user guide to modularization concepts and the ground-water flow procesS, Geological Survey. CO McDonald Morrissey Associates.
Henry, H.R., Kohout, F.A., 1972. Circulation patterns of saline groundwater affected by geothermal heating as related to waste disposal. In: Underground Water Management and Environmental Implications, Amer Assoc Pet Geol, Memoir 18, pp. 202-221.
Hopmans, J.W., Šimunek, J., Bristow, K.L., 2002. Indirect estimation of soil thermal properties and water flux using heat pulse probe measurements: Geometry and dispersion effects. Water Resour. Res. 38, 7-1-7–14. 10.1029/2000wr000071.
Hughes, J.D., Vacher, H.L., Sanford, W.E., 2007. Three-dimensional flow in the Florida platform: Theoretical analysis of Kohout convection at its type locality. Geology 35, 663–666. https://doi.org/10.1130/G23374A.1.
Ingebritsen, S.E., Sanford, W.E., 1998. Groundwater in Geologic Processes. Cambridge University Press, Cambridge, UK.
Jabaloy-Sánchez, A., Lobo, F.J., Azor, A., Martín-Rosales, W., Pérez-Peña, J.V., Bárcenas, P., Macías, J., Fernández-Salas, L.M., Vázquez-Vílchez, M., 2014. Six thousand years of coastline evolution in the Guadalfeo deltaic system (southern Iberian Peninsula). Geomorphology 206, 374–391. https://doi.org/10.1016/j.geomorph.2013.08.037.
Keery, J., Binley, A., Crook, N., Smith, J.W.N., 2007. Temporal and spatial variability of groundwater-surface water fluxes: Development and application of an analytical method using temperature time series. J. Hydrol. 336, 1–16. https://doi.org/10.1016/j.jhydrol.2006.12.003.
Kim, K.Y., Chon, C.M., Park, K.H., Park, Y.S., Woo, N.C., 2008. Multi-depth monitoring of electrical conductivity and temperature of groundwater at a multilayered coastal aquifer: Jeju Island, Korea. Hydrol. Process. 22, 3724–3733. https://doi.org/10.1002/hyp.6976.
Kim, K.Y., Park, Y.S., Kim, G.P., Park, K.H., 2009. Dynamic freshwater-saline water interaction in the coastal zone of Jeju Island, South Korea. Hydrogeol. J. 17, 617–629. https://doi.org/10.1007/s10040-008-0372-4.
Kinnear, J.A., Binley, A., Duque, C., Engesgaard, P.K., 2013. Using geophysics to map areas of potential groundwater discharge into Ringkøbing Fjord, Denmark. Lead. Edge. 32 https://doi.org/10.1190/tle32070792.1.
Kohout, F.A., 1965. Section of geological sciences: a hypothesis concerning cyclic flow of salt water related to geothermal heating in the Floridan aquifer. Trans. N. Y. Acad. Sci. 28, 249–271. https://doi.org/10.1111/j.2164-0947.1965.tb02879.x.
Kohout, F.A., 1967. Groundwater flow and the geothermal regime of the Floridan Plateau. Trans Gulf Coast Assoc Geol Soc 17, 339–354.
Kohout, F.A., Henry, H., Banks, J., 1977. Hydrogeology related to geothermal conditions of the Floridan Plateau. In: Smith D, Grien G (eds) The geothermal nature of the Floridan Plateau. Florida Dept Nat Resour Spec Publ 21 pp. 1-41.
Kohout, F.A., 1964. The flow of fresh water and salt water in the Biscayne aquifer of the Miami area, Florida. In: sea water in coastal aquifers: U.S.G.S. Water-Supply, 1613, 12– 32.
Kurylyk, B.L., Bourque, C.-P.-A., MacQuarrie, K.T.B., 2013. Potential surface temperature and shallow groundwater temperature response to climate change: an example from a small forested catchment in east-central New Brunswick (Canada). Hydrol. Earth Syst. Sci. Discuss. 10, 3283–3326. https://doi.org/10.5194/hessd-10-3283-2013.
Kurylyk, B.L., Irvine, D.J., Bense, V.F., 2019. Theory, tools, and multidisciplinary applications for tracing groundwater fluxes from temperature profiles. Wiley Interdiscip. Rev. Water 6, e1329. https://doi.org/10.1002/wat2.1329.
Langevin, C.D., Dausman, A.M., Sukop, M.C., 2010. Solute and heat transport model of the Henry and Hilleke laboratory experiment. Groundwater 48, 757–770. https://doi.org/10.1111/j.1745-6584.2009.00596.x.
Langevin, C.D., Thorne , D.T., Dausman, A.M., Sukop, M.C., Guo. W., 2007. SEAWAT Version 4: A Computer Program for Simulation of multi-species Solute and Heat Transport. U.S. Geological Survey Techniques and Methods. book 6, chap. A22 Reston, Virginia: USGS.
Langevin, C.D., Dausman, A.M., Thorne, D., Sukop., M.C., 2008. Modeling solute and heat transport with SEAWAT. In MODFLOW and More 2008: Ground Water and Public Policy–Conference Proceedings, Golden, Colorado, 19–21 May 2008.
Lautz, L.K., 2012. Observing temporal patterns of vertical flux through streambed sediments using time-series analysis of temperature records. J. Hydrol. 464–465, 199–215. https://doi.org/10.1016/j.jhydrol.2012.07.006.
Levanon, E., Shalev, E., Yechieli, Y., Gvirtzman, H., 2016. Advances in Water Resources Fluctuations of fresh-saline water interface and of water table induced by sea tides in unconfined aquifers. Adv. Water Resour. 96, 34–42. https://doi.org/10.1016/j.advwatres.2016.06.013.
Limberger, J., Boxem, T., Pluymaekers, M., Bruhn, D., Manzella, A., Calcagno, P., Beekman, F., Cloetingh, S., van Wees, J.D., 2018. Geothermal energy in deep aquifers: A global assessment of the resource base for direct heat utilization. Renew. Sustain. Energy Rev. 10.1016/j.rser.2017.09.084.
Liu, J., Du, J., Yu, X., 2021. Submarine groundwater discharge enhances primary productivity in the Yellow Sea, China: Insight from the separation of fresh and recirculated components. Geosci. Front. 12, 101204 https://doi.org/10.1016/j.gsf.2021.101204.
Ma, R., Zheng, C., Zachara, J.M., Tonkin, M., 2012. Utility of bromide and heat tracers for aquifer characterization affected by highly transient flow conditions. Water Resour. Res. 48 https://doi.org/10.1029/2011WR011281.
Manca, B., Burca, M., Giorgetti, A., Coatanoan, C., García, M.J., Iona, A. 2004. Physical and biochemical averaged vertical profiles in the Mediterranean regions: an important tool to trace the climatology of water masses and to validate incoming data from operational oceanography. 48, 83-116.
McCallum, A.M., Andersen, M.S., Rau, G.C., Larsen, J.R., Acworth, R.I., 2014. Investigated using point and reach measurements. Water Resour. Res. 2815–2829 https://doi.org/10.1002/2012WR012922.
Molina, L., Vallejos, A., Pulido-Bosch, A., Sánchez-Martos, F., 2002. Water temperature and conductivity variability as indicators of groundwater behaviour in complex aquifer systems in the south-east of Spain. Hydrol. Process. 16, 3365–3378. https://doi.org/10.1002/hyp.1105.
Molina-Giraldo, N., Bayer, P., Blum, P., 2011. Evaluating the influence of thermal dispersion on temperature plumes from geothermal systems using analytical solutions. Int. J. Therm. Sci. 50, 1223–1231. https://doi.org/10.1016/j.ijthermalsci.2011.02.004.
Panteli, N.M., 2018. Assessment of the effect of groundwater flow on the performance of Borehole Thermal Energy Storage systems. MS thesis, Delft University of Technology, 59 p.
Park, B.H., Bae, G.O., Lee, K.K., 2015. Importance of thermal dispersivity in designing groundwater heat pump (GWHP) system: Field and numerical study. Renew. Energy 83, 270–279. https://doi.org/10.1016/j.renene.2015.04.036.
Parsons, M.L., 1970. Groundwater thermal regime in a glacial complex. Water Resour. Res. 6, 1701–2172.
Piga, B., Casasso, A., Pace, F., Godio, A., Sethi, R., 2017. Thermal impact assessment of groundwater heat pumps (GWHPs): Rigorous vs. simplified models. Energies 10. https://doi.org/10.3390/en10091385.
Pollack, H.N., Huang, S., 2000. Climate reconstruction from subsurface temperatures. Annu. Rev. Earth Planet. Sci. 28, 339–365. https://doi.org/10.1146/annurev.earth.28.1.339.
Pollack, H.N., Smerdon, J.E., van Keken, P.E., 2005. Variable seasonal coupling between air and ground temperatures: A simple representation in terms of subsurface thermal diffusivity. Geophys. Res. Lett. 32 https://doi.org/10.1029/2005GL023869.
Ranjan, S.P., Kazama, S., Sawamoto, M., 2004. Modeling of the dynamics of saltwater–freshwater, interface in coastal aquifers. In: Proceedings of the joint AOGS annual meeting & APHW second conference. Singapore. 373–380.

Rushton, K., 2007. Representation in regional models of saturated river-aquifer interaction for gaining/losing rivers. J. Hydrol. 334, 262–281. 10.1016/j.jhydrol.2006.10.008.

Sánchez-Úbeda, J.P., López-Chicano, M., Calvache, M.L., Purtschert, R., Engesgaard, P., Martín-Montañés, C., Sültenfuβ, J., Duque, C., 2018b. Groundwater Age Dating in Motril-Salobreña Coastal Aquifer with Environmental Tracers (δ18O/δ2H, 3H/3He, 4He, 85Kr, and 39Ar). In: Calvache M., Duque C., Pulido-Velazquez D. (eds) Groundwater and Global Change in the Western Mediterranean Area. Environ. Earth Sci. Springer, Cham. 10.1007/978-3-319-69356-9_33.

Sánchez-Úbeda, J.P., Calvache, M.L., Engesgaard, P., Duque, C., López-Chicano, M., Purtschert, R., 2018a. Numerical Modeling of Groundwater Age Distribution in Motril-Salobreña Coastal Aquifer (SE Spain). In: Calvache M., Duque C., Pulido-Velazquez D. (eds) Groundwater and Global Change in the Western Mediterranean Area. Environ. Earth Sci. Springer, Cham. doi: 10.1007/978-3-319-69356-9_32.

Schärli, U., Rybach, L., 2001. Determination of specific heat capacity on rock fragments. Geothermics 30 (1), 93–110. https://doi.org/10.1016/S0375-6505(00)00035-3.

Sebok, E., Duque, C., Engesgaard, P., Boegh, E., 2015. Application of Distributed Temperature Sensing for coupled mapping of sedimentation processes and spatio-temporal variability of groundwater discharge in soft-bedded streams. Hydrol. Process. 29, 3408–3422. https://doi.org/10.1002/hyp.10455.

Shalev, E., Lazar, A., Wollman, S., Kington, S., Yechieli, Y., Gvirtzman, H., 2009. Biased monitoring of fresh water-salt water mixing zone in coastal aquifers. Ground Water 47, 49–56. https://doi.org/10.1111/j.1745-6584.20 08.0 0502.x.

Silliman, S.E., Booth, D.F., 1993. Analysis of time-series measurements of sediment temperature for identification of gaining vs. losing portions of Juday Creek, Indiana. J. Hydrol. 146, 131–148. https://doi.org/10.1016/0022-1694(93)90273-C.

Smerdon, J.E., Pollack, H.N., Enz, J.W., Lewis, M.J., 2003. Conduction-dominated heat transport of the annual temperature signal in soil. J. Geophys. Res. Solid Earth 108. https://doi.org/10.1029/2002jb002351.

Smith, L., Chapman, D.S., 1983. On the thermal effects of groundwater flow 1. Regional scale systems. J. Geophys. Res. 88, 593–608. https://doi.org/10.1029/JB088iB01p00593.

Stallman, R.W., 1965. Steady one-dimensional fluid flow in a semi-infinite porous medium with sinusoidal surface temperature. J. Geophys. Res. 70 (12), 2821–2827. https://doi.org/10.1029/JZ070i012p02821.

Stallman, R.W., 1963. Computation of ground-water velocity from temperature data. In: Methods of Collecting and Interpreting Ground-Water Data, ed. R. Bentall, 36–46. Water Supply Paper 1544-H. Washington, DC: USGS.

Stauffer, F., Bayer, P., Blum, P., Giraldo, N., Kinzelbach, W., 2014. Thermal Use of Shallow Groundwater. Boca Raton: CRC Press, 10.1201/b16239.

Stein, S., Sola, F., Yechieli, Y., Shalev, E., Sivan, O., Kasher, R., Vallejos, A., 2020. The effects of long-term saline groundwater pumping for desalination on the fresh – saline water interface: field observations and numerical modeling. Sci. Total Environ. 732, 139249 https://doi.org/10.1016/j.scitotenv.2020.139249.

Suzuki, S., 1960. Percolation measurements based on heat flow through soil with special reference to paddy fields. J. Geophys. Res. 65, 2883–2885. https://doi.org/10.1029/JZ065i009p02883.

Szijártó, M., Galsa, A., Tóth, Á., Mádl-Szőnyi, J., 2019. Numerical investigation of the combined effect of forced and free thermal convection in synthetic groundwater basins. J. Hydrol. 572, 364–379. https://doi.org/10.1016/j.jhydrol.2019.03.003.

Taniguchi, M., 2000. Evaluations of the saltwater-groundwater interface from borehole temperatura in a coastal region. Geophys. Res. Lett. 27, 713–716.

Taniguchi, M., Shimada, J., Tanaka, T., Kayane, I., Sakura, Y., Shimano, Y., Dapaah-Siakwan, S., Kawashima, S., 1999. Disturbances of temperature-depth profiles due to surface climate change and subsurface water flow: 1. An effect of linear increase in surface temperature caused by global warming and urbanization in the Tokyo metropolitan area, Japan. Water Resour. Res. 35, 1507–1517. https://doi.org/10.1029/1999WR900009.

Thorne, D., Langevin, C.D., Sukop, M.C., 2006. Addition of simultaneous heat and solute transport and variable fluid viscosity to SEAWAT. Comput. Geosci. 32, 1758–1768. https://doi.org/10.1016/j.cageo.2006.04.005.

Tirado-Conde, J., Engesgaard, P., Karan, S., Müller, S., Duque, C., 2019. Evaluation of temperature profiling and seepage meter methods for quantifying submarine groundwater discharge to coastal lagoons: impacts of saltwater intrusion and the associated thermal regime. Water. 11, 1648. https://doi.org/10.3390/w11081648.

Tóth, J., 1962. A theory of groundwater motion in small basins in central Alberta. Canada. J. Geophys. Res. 67, 4375–43787. https://doi.org/10.1029/JZ067i011p04375.

Vandenbohede, A., Lebbe, L., 2011. Heat transport in a coastal groundwater flow system near De Panne, Belgium. Hydrogeol. J. 19, 1225–1238. https://doi.org/10.1007/s10040-011-0756-8.

Vandenbohede, A., Louwyck, A., Lebbe, L., 2009. Conservative solute versus heat transport in porous media during push-pull tests. Transp. Porous Media 76, 265–287. https://doi.org/10.1007/s11242-008-9246-4.

Vandenbohede, A., Van Houtte, E., 2012. Heat transport and temperature distribution during managed artificial recharge with surface ponds. J. Hydrol. 472–473, 77–89. https://doi.org/10.1016/j.jhydrol.2012.09.028.

Walther, M., Graf, T., Kolditz, O., Liedl, R., Post, V., 2017. How significant is the slope of the sea-side boundary for modelling seawater intrusion in coastal aquifers? J. Hydrol. 551, 648–659. https://doi.org/10.1016/j.jhydrol.2017.02.031.

Woodbury, A.D., Smith, L., 1988. Simultaneous inversion of hydrogeologic and thermal data, 2. Incorporation of thermal data. Water Resour. Res. 23, 356–372. https://doi.org/10.1029/WR024i003p00356.

Xiaoqing, S., Ming, J., Peiwen, X., 2018. Analysis Of The Thermophysical Properties And Influencing Factors Of Various Rock Types From The Guizhou Province, in: E3S Web of Conferences. EDP Sciences. 10.1051/e3sconf/20185303059.

Zhang, Y., Li, H., Guo, H., Zheng, C., Wang, X., Zhang, M., Xiao, K., 2020. Improvement of evaluation of water age and submarine groundwater discharge: a case study in Daya Bay, China. J. Hydrol. 586, 124775 https://doi.org/10.1016/j.jhydrol.2020.124775.

Zheng, C., Wang., P.P., 1999. MT3DMS—A modular three-dimensional multispecies transport model for simulation of advection, dispersion and chemical reactions of contaminants in groundwater systems: Documentation and user's guide. U.S. Army Corps of Engineers Contract Report SERDP-99-1.